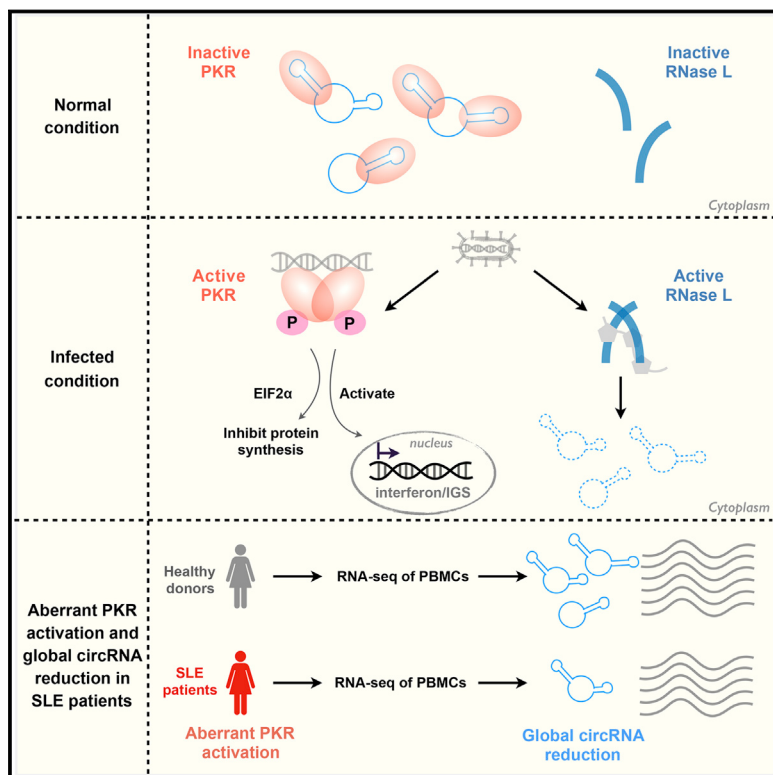


Structure and Degradation of Circular RNAs Regulate PKR Activation in Innate Immunity

Graphical Abstract



Authors

Chu-Xiao Liu, Xiang Li, Fang Nan, ..., Nan Shen, Li Yang, Ling-Ling Chen

Correspondence

nanshensibs@gmail.com (N.S.), liyang@picb.ac.cn (L.Y.), linglingchen@sibcb.ac.cn (L.-L.C.)

In Brief

The unique structure of circRNAs allows them to bind and regulate the innate immune dsRNA receptor PKR, and misregulation of this process is found in patients with autoimmune disease.

Highlights

- circRNAs are globally degraded by activated RNase L upon viral infection
- Many circRNAs tend to form 16–26 bp duplexes and act as endogenous PKR inhibitors
- The RNase L-mediated circRNA degradation is required for PKR activation
- circRNA reduction and aberrant PKR activation are found in autoimmune disease SLE

Structure and Degradation of Circular RNAs Regulate PKR Activation in Innate Immunity

Chu-Xiao Liu,^{1,7} Xiang Li,^{1,7} Fang Nan,^{2,7} Shan Jiang,¹ Xiang Gao,^{1,3} Si-Kun Guo,¹ Wei Xue,² Yange Cui,⁴ Kaige Dong,² Huihua Ding,⁵ Bo Qu,⁵ Zhaocai Zhou,¹ Nan Shen,^{4,5,6,*} Li Yang,^{2,3,*} and Ling-Ling Chen^{1,3,8,*}

¹State Key Laboratory of Molecular Biology, Shanghai Key Laboratory of Molecular Andrology, CAS Center for Excellence in Molecular Cell Science, Shanghai Institute of Biochemistry and Cell Biology, University of Chinese Academy of Sciences, Chinese Academy of Sciences, 320 Yueyang Road, Shanghai 200031, China

²CAS Key Laboratory of Computational Biology, CAS-MPG Partner Institute for Computational Biology, Shanghai Institute of Nutrition and Health, Shanghai Institutes for Biological Sciences, University of Chinese Academy of Sciences, Chinese Academy of Sciences, 320 Yueyang Road, Shanghai 200031, China

³School of Life Science and Technology, ShanghaiTech University, 100 Haik Road, Shanghai 201210, China

⁴Laboratory of Molecular Rheumatology, Shanghai Institute of Nutrition and Health, Shanghai Institutes for Biological Sciences, University of Chinese Academy of Sciences, Chinese Academy of Sciences, 320 Yueyang Road, Shanghai 200031, China

⁵Shanghai Institute of Rheumatology, China-Australia Centre for Personalized Immunology, Renji Hospital, School of Medicine, Shanghai Jiao Tong University, Shanghai, China

⁶Center for Autoimmune Genomics and Etiology, Cincinnati Children's Hospital Medical Center, Department of Pediatrics, University of Cincinnati College of Medicine, Cincinnati, OH, USA

⁷These authors contributed equally

⁸Lead Contact

*Correspondence: nanshensibs@gmail.com (N.S.), liyang@picb.ac.cn (L.Y.), linglingchen@sibcb.ac.cn (L.-L.C.)

<https://doi.org/10.1016/j.cell.2019.03.046>

SUMMARY

Circular RNAs (circRNAs) produced from back-splicing of exons of pre-mRNAs are widely expressed, but current understanding of their functions is limited. These RNAs are stable in general and are thought to have unique structural conformations distinct from their linear RNA cognates. Here, we show that endogenous circRNAs tend to form 16–26 bp imperfect RNA duplexes and act as inhibitors of double-stranded RNA (dsRNA)-activated protein kinase (PKR) related to innate immunity. Upon poly(I:C) stimulation or viral infection, circRNAs are globally degraded by RNase L, a process required for PKR activation in early cellular innate immune responses. Augmented PKR phosphorylation and circRNA reduction are found in peripheral blood mononuclear cells (PBMCs) derived from patients with autoimmune disease systemic lupus erythematosus (SLE). Importantly, overexpression of the dsRNA-containing circRNA in PBMCs or T cells derived from SLE can alleviate the aberrant PKR activation cascade, thus providing a connection between circRNAs and SLE.

INTRODUCTION

A large number of circular RNAs (circRNAs) produced from precursor mRNA (pre-mRNA) back-splicing of exon(s) have been identified in eukaryotes. They are generally expressed at low levels and often exhibit cell-type- and tissue-specific patterns. Recent studies have shown that their biogenesis requires spli-

ceosomal machinery and can be modulated by both intronic complementary sequences (ICs) and RNA binding proteins (RBPs). Functions of most circRNAs remain largely unexplored, but at the molecular level, some are involved in sequestration of microRNAs or proteins, modulation of transcription, interference with splicing, and translation to produce polypeptides (for reviews, see Li et al. [2018] and Wilusz [2018]). However, considering the generally low efficiency of back-splicing (<1% of canonical splicing) in cells (Zhang et al., 2016b), the functional potential of most individual circRNAs remains elusive.

It has been recently shown that circRNAs are likely associated with innate immune responses. On the one hand, transfection of *in vitro*-generated circRNAs into mammalian cells led to potent induction of innate immunity genes including the pattern recognition receptor RIG-I (retinoic acid inducible gene I) that confers protection against viral infection and elicit immune responses (Chen et al., 2017), although how the exogenous circRNA is recognized by RIG-I remains unclear. On the other hand, the biogenesis of nascent circRNAs was reduced upon viral infection due to the enhanced nucleocytoplasmic export of the immune factors NF90/NF110 that normally bind to ICs to promote circRNA formation (Li et al., 2017). Furthermore, upregulated circRNA expression via expression plasmids introduced into human cells facilitated viral infection (Li et al., 2017). This latter observation was consistent with a recent finding that cellular accumulation of RNA lariat circles caused by autosomal recessive debranching enzyme DBR1 deficiency resulted in patient susceptibility to severe viral infections of the brainstem (Zhang et al., 2018). Together, these recent studies point to the view that circRNAs are involved in innate immunity regulation, but how they act in this important context remains to be explored.

Innate immunity relies on different immune receptors to detect characteristic pathogens, including receptors that are specialized in the detection of foreign nucleic acids as the dominant

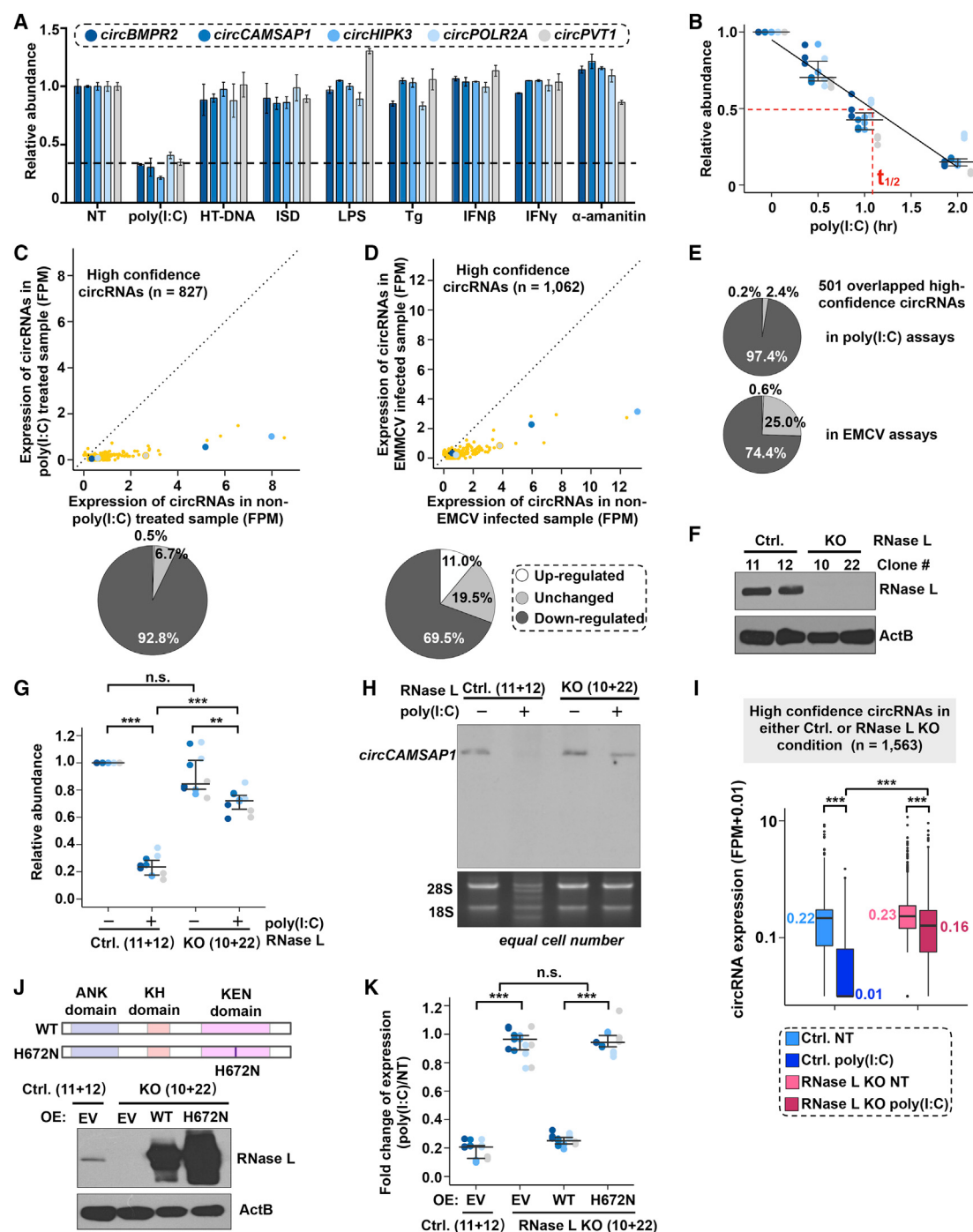


Figure 1. circRNAs Are Degraded by RNase L upon poly(I:C) or EMCV Treatment

(A) circRNAs are degraded upon poly(I:C) treatment. Poly(I:C) (1 μ g/mL), HT-DNA (5 μ g/mL), or ISD (5 μ g/mL) was transfected into HeLa cells for 6 h; LPS (300 ng/mL), Tg (3 μ M), IFN β (2,000 U/mL), IFN γ (2,000 U/mL), or α -amanitin (2 μ g/mL) was added to the medium for 6 h, followed by detection of circRNA abundance by qRT-PCR.

(B) circRNA half-life upon poly(I:C) treatment. The relative abundance of each circRNA shown in (A) was measured upon poly(I:C) transfection at indicated time points.

(C and D) Global reduction of high confidence circRNAs ($FPM \geq 0.2$) upon poly(I:C) for 6 h (C) or EMCV for 24 h (D). Top: scatterplots showing high-confidence circRNA expression between untreated and poly(I:C)-treated (C) or EMCV-infected cells (D). circRNAs shown in (A) were highlighted. Bottom: pie charts showing upregulated (fold change ≥ 2), unchanged (fold change > 0.05 and < 2), and downregulated (fold change ≤ 0.5) high-confidence circRNAs.

(E) Expression of overlapped high-confidence circRNAs shown in (C) and (D) was decreased upon poly(I:C) (top) or EMCV (bottom) treatments. See above for details.

(legend continued on next page)

antiviral defense pathway in vertebrates (Schlee and Hartmann, 2016). Multiple complementary and independent systems have been implicated in responses to pathogenic double-stranded RNA (dsRNA) activity, including two major categories of nucleic acid receptors. The first category comprises pattern recognition receptors such as the helicases MDA5 (melanoma differentiation associated protein 5), RIG-I, and the Toll-like receptor 3 (TLR3), which recognize different biochemical features of foreign nucleic acids and induce immune responses via activating transcription factors and cytokines. The second category of receptors comprises nucleic acid receptors with direct antiviral activity, e.g., PKR (dsRNA-activated protein kinase), the 2'-5' oligoadenylate synthetase [OAS] and RNase L, and adenosine deaminase acting on RNA 1 (ADAR1). The latter group of proteins recognizes dsRNAs of different length; they directly act on viral RNA by inhibiting translation, by triggering degradation, or by chemical modification of pathogenic dsRNAs (Schlee and Hartmann, 2016).

Given that circRNAs contain sequences almost entirely identical to those of their linear cognate RNAs, challenges exist at multiple levels to understand their regulation and functions (Li et al., 2018). circRNAs are thought to have two unique features that linear RNAs may lack. First, they are stable due to their circularity and resistance to the cellular linear RNA decay machineries. So far, little is known how circRNAs are degraded in cells. Second, the circular feature may endow circRNAs with unique structural conformations to distinguish them from linear RNAs. However, the detection of circRNA structures has been hindered by largely overlapping sequences between circRNAs and their linear cognate RNAs.

In the current study, by addressing how circRNAs are degraded and structured, we show that many examined circRNAs tend to form 16–26 base pair (bp) intra-molecularly imperfect RNA duplexes (intra-dsRNAs). circRNAs preferentially bind to PKR and act as endogenous PKR inhibitors. They undergo massive and rapid degradation by RNase L, a process that is required for PKR activation in the early stage of innate immune response and that is linked to the autoimmune disease systemic lupus erythematosus (SLE).

RESULTS

circRNAs Are Significantly Downregulated in Cells upon Poly(I:C) Treatment or Viral Infection

As circRNAs are stable in examined cells and tissues under normal conditions (Enuka et al., 2016; Zhang et al., 2016b), we

sought to examine whether they could be degraded upon certain cellular stresses. HeLa cells were treated with a number of stressors followed by the examination of steady-state level of several highly and universally expressed circRNAs (Figure S1). We found that stimulation with poly(I:C), widely used to mimic pathogenic dsRNAs or viral infection, led to dramatic and rapid reduction of all examined circRNAs (Figure 1A) with a turnover half-life of ~1 h (Figure 1B). Previous metabolic labeling of nascent circRNAs revealed that back-splicing efficiency is <1% of canonical splicing (Zhang et al., 2016b). Consistent with this notion, addition of α -amanitin to stop RNA polymerase II transcription did not affect the level of examined circRNAs (Figure 1A). Further treatment of poly(I:C) to the α -amanitin-treated cells still led to rapid and dramatic circRNA degradation (Figure S2A). Thus, the observed fast turnover (Figure 1B) of circRNAs upon poly(I:C) treatment was not due to the transcriptional level interference, but degradation. Such degradation was specific to poly(I:C), as other tested treatments, such as herring testes DNA (HT-DNA) and IFN-stimulating DNA (ISD) mimicking dsDNA stimulation, lipopolysaccharide (LPS) and thapsigargin (Tg) mimicking bacterial infection, and interferon (IFN)- β or IFN- γ as inflammatory cytokines, had little effect on circRNA stability (Figure 1A). In addition, the poly(I:C)-induced circRNA reduction was also observed in other human cells including PA1, THP1, and Jurkat cells (Figure S2B). Such a rapid reduction of circRNAs was genome-wide upon poly(I:C) stimulation (Figures 1C and S2C; Table S1) and in HeLa cells infected with the RNA virus, encephalomyocarditis (EMCV) (Figures 1D and S2D; Table S2). Importantly, most circRNAs were found to be reduced in both poly(I:C)- and EMCV-treated cells (Figures 1E, S2E, and S2F; Table S3), highlighting the view that both poly(I:C) and viral dsRNAs can trigger global circRNA degradation.

Genome-wide circRNA Degradation by RNase L upon Poly(I:C) Treatment or Viral Infection

How are circRNAs degraded in cells upon viral infection? It is known that oligoadenylate synthetase (OAS) is activated upon binding to pathogenic dsRNA to produce 2',5'-linked oligoadenylates (2-5A) of variable length from ATP (Schlee and Hartmann, 2016). RNase L, a widely expressed cytoplasmic endoribonuclease, dimerizes and is activated by 2-5A. Activated RNase L then catalyzes the degradation of viral and cellular RNAs as one way to limit virus spread (Han et al., 2014; Huang et al., 2014). Of note, it has been reported that both poly(I:C) and EMCV can activate RNase L (Huang et al., 2014). Based on these early findings, we hypothesized that RNase L may be

(F) Generation of RNase L knockout (KO) HeLa cell lines by CRISPR/Cas9, confirmed by western blotting (WB). To limit the heterogeneity between single cell clones, two control or KO lines were mixed respectively for experiments carried out in Figures 1G–1K, 5H, S2I, S3E, S6K, and S7F.

(G) Poly(I:C)-triggered circRNAs degradation was rescued by RNase L KO, shown by qRT-PCR.

(H) Poly(I:C)-triggered circCAMSAP1 degradation was rescued by RNase L KO, shown by NB. Of note, rRNAs were degraded in control cells treated with poly(I:C) as reported (Han et al., 2014).

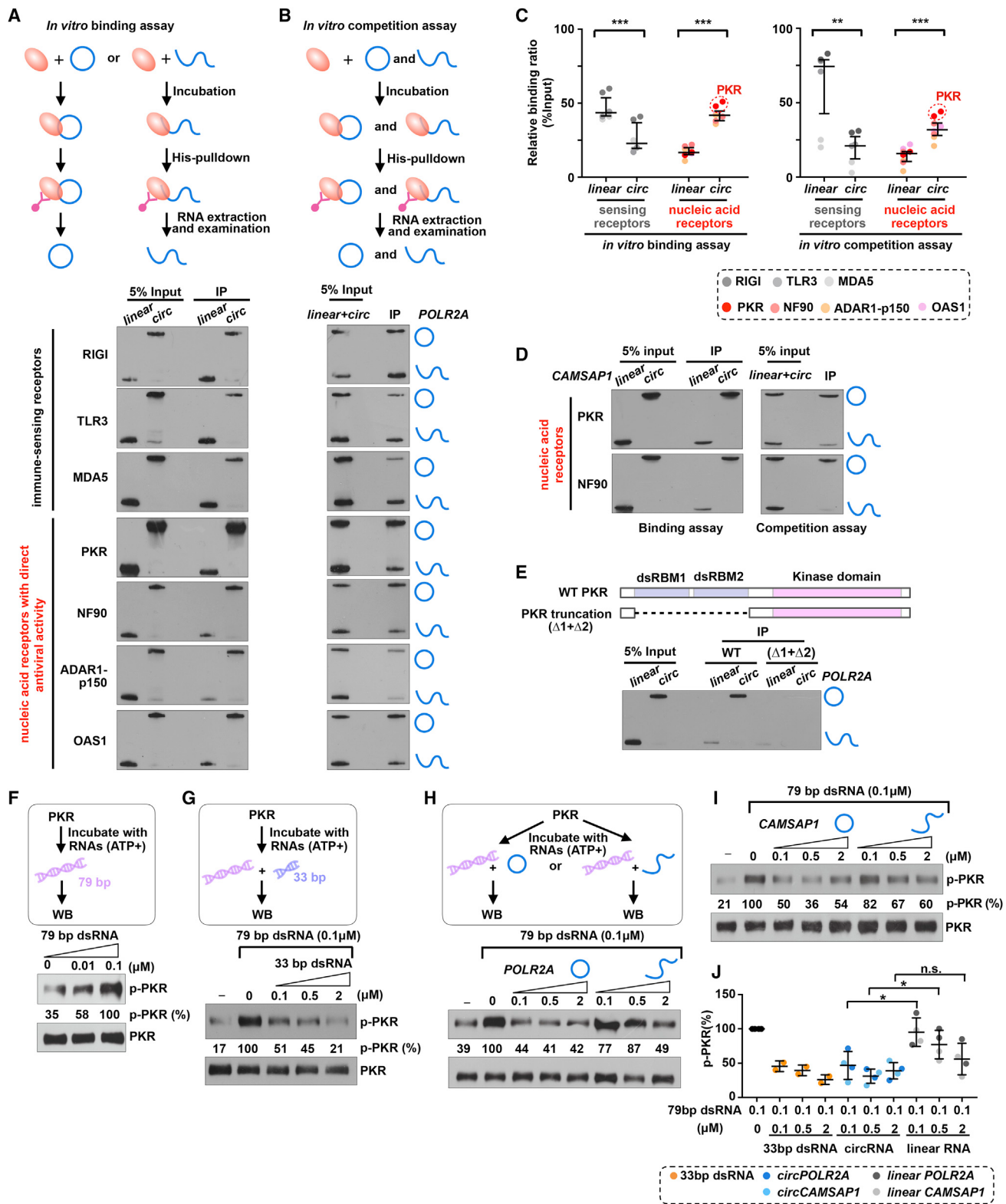
(I) RNase L is responsible for global circRNA degradation in cells treated with poly(I:C). High confidence circRNAs were selected by FPM ≥ 0.2 in at least one sample. The median, IQR, and $1.5 \times$ IQR are shown. Wilcoxon rank-sum test, ***p < 0.001.

(J) Top: a schematic drawing of RNase L (WT) and its nuclease-dead mutation (H672N). Bottom: WB confirmed overexpression of WT or H672N in RNase L KO HeLa cells. EV, empty vector.

(K) The endonuclease activity of RNase L is required for circRNA degradation.

(A and B) Error bars represent SD. (G and K), Data are shown as median and IQR. n.s., p > 0.05, **p < 0.01, ***p < 0.001, Student's t test.

See also Figures S1, S2, and S3 and Tables S1, S2, S3, S4, and S5.



(legend on next page)

responsible for the observed circRNA degradation upon poly(I:C) and viral stimulations.

To test this possibility, we generated RNase L knockout (KO) by CRISPR/Cas9 (Figure 1F) and knockdown (KD) by short hairpin RNAs (shRNAs) (Figure S2G) HeLa cells. Upon poly(I:C) treatment, the reduction of all examined circRNAs was largely eliminated in both RNase L KO (Figure 1G) and KD (Figure S2H) cells, and the reduction of *circCAMSAP1* was further confirmed by northern blot (NB) (Figure 1H). Genome-wide analyses revealed that RNase L KO had no effect on circRNA expression under normal conditions (Figure S2I), while the global reduction of circRNAs by RNase L upon poly(I:C) stimulation (Figures 1C and S2C; Table S1) was largely diminished in RNase L KO cells (Figure 1I; Table S4). It should be noted that RNase L KO did not fully rescue the loss of circRNAs during poly(I:C) stimulation (Figures 1G–1I). This is because viral infection also inhibits the biogenesis of nascent circRNAs (Li et al., 2017), in addition to their degradation. Importantly, re-introduction of wild type (WT) or inactive (H672N) (Han et al., 2014) RNase L into KO (Figure 1J) or KD (Figure S2J) cells followed by poly(I:C) treatment showed that the catalytic activity of RNase L was essential for circRNA degradation (Figures 1K and S2K). Finally, transfection of synthetic 2'-SA to directly activate RNase L (Han et al., 2014) also led to robust degradation of circRNAs (Figure S2L). Collectively, these findings reveal that RNase L is the key enzyme for circRNA degradation upon viral infection.

Cellular mRNAs were also cleaved upon RNase L activation, as linear RNAs were reduced upon poly(I:C) (Figure S3A; Table S1) or EMCV (Figure S3B; Table S2) treatments. Interestingly, compared to 10%–30% loss of linear RNAs (Figures S3A and S3B), 80%–90% circRNAs were efficiently removed upon poly(I:C) or EMCV treatments (Figures 1C, 1D, S2C, and S2D). Such a robust reduction of circRNAs over linear cognate RNAs was at least in part owing to inefficient back-splicing in cells (Zhang et al., 2016b), which limited the amount of nascent circRNAs produced from pre-mRNAs to supplement their rapid degradation by RNase L (Figure S3C). Of note, MTT assays showed that cells remained 100% or 80% viable within 2 or 6 h of poly(I:C) treatment (Figure S3D). Dead cells were washed

off prior to RNA isolation for RNA sequencing (RNA-seq), therefore results obtained from the subsequent RNA-seq were likely unaffected. In addition, only marginal reduction of circular and linear RNAs (Figures 1I and S3E; Table S4) was observed in RNase L KO cells upon poly(I:C) treatment. All these controls exclude the possibility of cellular toxicity-mediated RNA degradation.

circRNAs Prefer to Bind PKR and Regulate PKR Activation *In Vitro*

Next, does this massive and rapid circRNA degradation play a role in innate immunity against pathogenic dsRNAs? One possibility is that circRNAs may bind to immune sensors and/or nucleic acid receptors to block their activation in normal situations. Upon viral invasion, RNase L-mediated circRNA degradation could then release these immune factors for function.

To identify circRNA-associated proteins, we performed both *in vitro* binding and competition screening assays (Figures 2A and 2B, top) with a number of purified immune factors tagged with histidine as well as purified linear and *in vitro* circularized RNAs with the same sequences from *circPOLR2A* (Figure S4A). Both assays (Figures 2A, 2B, and S4B) revealed that examined immune-sensing receptors including TLR3, RIG-I, and MDA5 preferred to bind linear *POLR2A*, while nucleic acid receptors with direct antiviral activity including PKR, NF90, ADAR1-p150, and OAS1 preferentially bound to *circPOLR2A*. Overall, although all examined proteins could bind both types of RNAs *in vitro* (Figures 2A, 2B, and S4B), quantification clearly showed that the examined circRNA, *circPOLR2A*, preferentially interacted with examined nucleic acid receptors, with the highest preference for PKR (Figure 2C). Similar results were found using another circRNA, *circCAMSAP1* (Figure 2D). *In vitro* binding assays with truncated proteins without dsRNA-binding motifs (dsRBMs) revealed that dsRBMs in PKR (Figure 2E) and NF90 (Figure S4C) were critical for their association with circRNAs.

PKR is an IFN-inducible Ser/Thr protein kinase that is directly activated by dsRNA, playing a central role in the cytoplasmic response to dsRNA. PKR is normally present in an unphosphorylated and inactive form in the cytoplasm and is activated upon

Figure 2. circRNAs Preferentially Bind to PKR and Prevent PKR Activation *In Vitro*

- (A) circRNAs prefer to bind to nucleic acid receptors with antiviral activity, shown by *in vitro* binding assays. Top: an illustration of the assay. Bottom: *in vitro* binding assays followed by examining each protein associated linear or circular *POLR2A* by NB on denaturing PAGE gels. Note that circular RNAs migrate much more slowly than their linear cognates with the same sequences on denaturing PAGE gels.
- (B) circRNAs prefer to bind to nucleic acid receptors with antiviral activity, shown by *in vitro* competition assays.
- (C) Quantification of *in vitro* binding and competition assays shown in (A), (B), and Figure S4B. Data are shown as median and IQR. ** $p < 0.01$, *** $p < 0.001$, Student's t test.
- (D) *CircCAMSAP1* preferentially binds to PKR and NF90, as revealed by both *in vitro* binding (left) and competition (right) assays.
- (E) dsRBMs of PKR are required for binding to *circPOLR2A*. Top: a schematic of PKR and the PKR truncation lacking both dsRBMs. Bottom: this PKR truncation was no longer associated with *circPOLR2A* as shown by the *in vitro* binding assay.
- (F) PKR is activated by 79 bp dsRNAs *in vitro*. PKR phosphorylation (p-PKR-T446, p-PKR for simplicity) was induced by 79 bp dsRNAs in a concentration-dependent manner, shown by WB.
- (G) 33 bp dsRNAs impair PKR phosphorylation *in vitro*. p-PKR by 79 bp dsRNAs (0.1 μ M) was blocked by the addition of 33 bp dsRNAs.
- (H) *CircPOLR2A*, but not its linear isoform, inhibits PKR phosphorylation *in vitro*. p-PKR by 79 bp dsRNAs (0.1 μ M) was blocked by addition of *in vitro* circularized and purified *circPOLR2A* but not the same amounts of linear *POLR2A* with the same sequences.
- (I) *CircCAMSAP1*, but not its linear isoform, inhibits PKR phosphorylation *in vitro*. The experiment was performed as shown in (H).
- (J) Quantification of results shown in (G)–(I) from duplicated assays. Images were quantified by Quantity One in individual assays and p-PKR levels were normalized by PKR expression in (F)–(I). Each dot represents results from one assay at the indicated concentration. * $p < 0.05$, n.s., $p > 0.05$, Student's t test. Data are shown as median and IQR.

See also Figure S4.

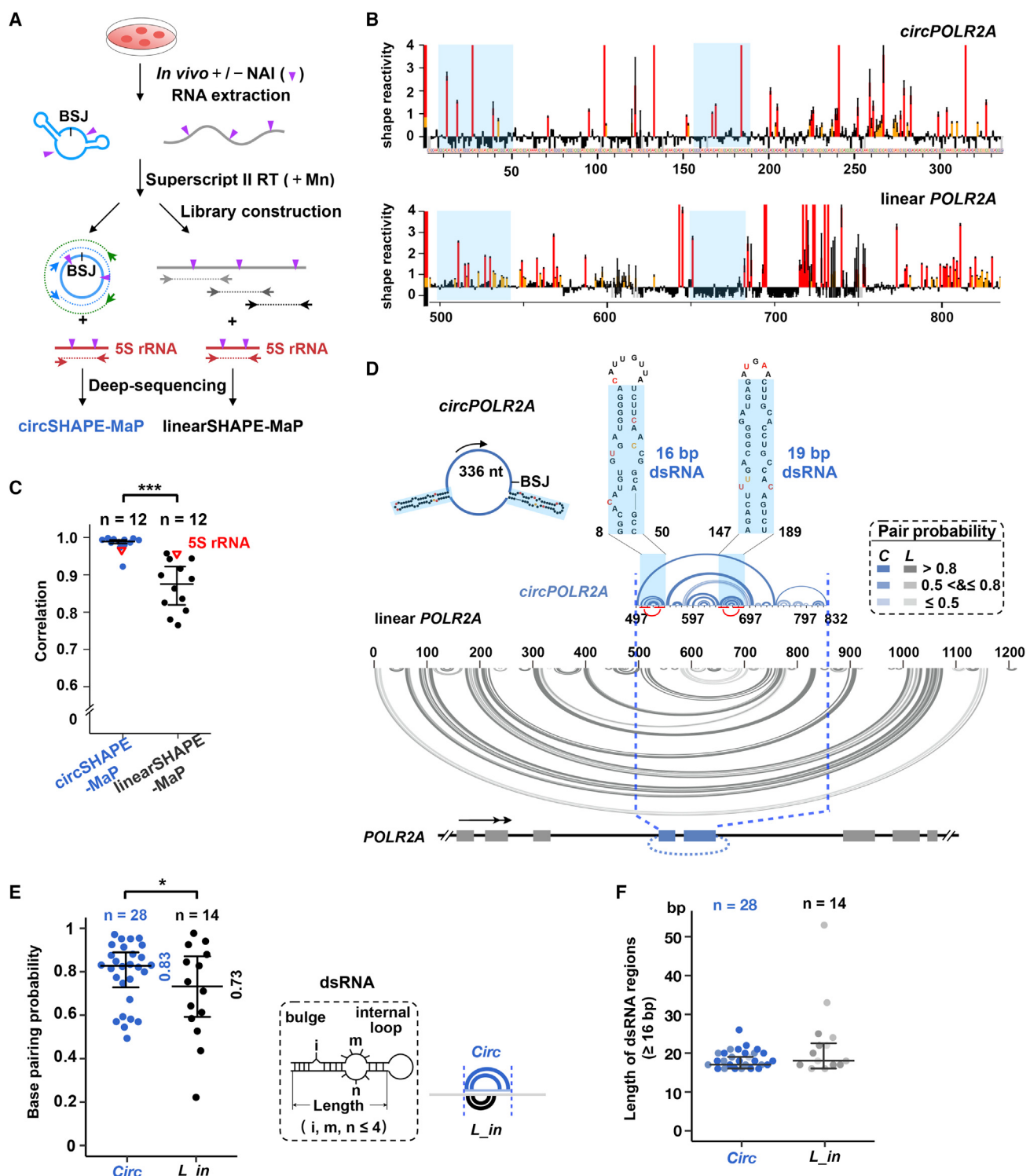


Figure 3. circRNAs Have Distinct Structural Conformation from Their Linear Cognate RNAs

(A) An illustration of SHAPE-MaP assays for circRNAs and their linear cognates.

(B) SHAPE-MaP profiles of *circPOLR2A* (top) and linear *POLR2A* (bottom). Blue shadows indicate the two RNA duplexes shown in (D).

(C) Correlation of biological replicates of SHAPE profiles of circRNAs is higher than their cognate linear RNAs. Spearman's rank correlation coefficient between biological replicates of 12 pairs of circRNAs (blue dots) and linear cognate RNAs (black dots). Note that the coefficient of 5S rRNA is high in both circSHAPE-MaP and linearSHAPE-MaP assays. *** $p < 0.001$, Student's t test.

(legend continued on next page)

infection by self-phosphorylation to initiate a signal transduction cascade that ultimately leads to inhibition of protein synthesis (Taylor et al., 2005) and induction of IFN (Pham et al., 2016). It has been reported that PKR activation requires long dsRNAs (>33 bp) with 79 bp achieving max-activation; however, short dsRNAs of 16–33 bp in length can bind PKR monomer and block its activation *in vitro* (Nallagatla et al., 2011; Zheng and Bevilacqua, 2004).

Considering the central role of PKR in the cytoplasmic response to dsRNA, we asked whether such a strong interaction of circRNA, rather than its linear cognate RNA, with PKR could regulate PKR activation. Consistent with previous studies, incubation of 79 bp long dsRNAs with PKR achieved dramatic PKR phosphorylation at 0.1 μ M concentration (Figure 2F); further addition of the same amount of 33 bp short dsRNAs (0.1 μ M) blocked this activation (Figure 2G). Strikingly, the addition of *in vitro* purified *circPOLR2A* (0.1 μ M) or *circCAMSAP1* (0.1 μ M), but not purified linear cognate RNAs (0.1 μ M) with the same sequences, achieved a comparable repression of PKR phosphorylation as by 33 bp dsRNAs (Figure 2H).

circRNAs Tend to Form 16–26 bp Imperfect RNA Duplexes in Cells

How do these RNA circles bind to PKR and regulate its activation? It is possible that circRNAs might have special topological structures to distinguish themselves from their linear cognate RNAs, likely forming intramolecular RNA duplexes, which allow their binding to dsRNA-binding proteins.

We optimized SHAPE-MaP (selective 2'-hydroxyl acylation analyzed by primer extension and mutational profiling) assays (Smola et al., 2015) for the comparison of paired circular (circSHAPE-MaP) and linear (linearSHAPE-MaP) RNA (Figure 3A) structures. For each pair, two sets of divergent primers crossing the back-splicing junctions (BSJs) for circRNAs and multiple sets of convergent primers for linear RNAs spanning circRNA-forming and non-circRNA forming exons were designed (Figures 3A and S5A–S5C; Table S5). 12 pairs of circular and linear RNAs yielded reliable SHAPE-MaP signals for comparison (Figures S5A and S5B). These circRNAs are expressed in multiple cell lines and contain moderate lengths from 150–450 nt for a full coverage of structure detection. Duplicate assays were performed with human 5S rRNA as an internal control in both circular and linear RNA SHAPE-MaP assays (Figures 3A and S5A–S5C). NAI (2-methylnicotinic acid imidazolidine) probing in cells gave rise to consistent and reliable signals for SHAPE-MaP assays with ~300 bp long tilling PCR products for both circular and linear RNAs (Figure S5B), using *circPOLR2A* and its paired linear

cognate RNA as an example (Figure 3B). An in-house pipeline was developed according to published methods (Busan and Weeks, 2018; Smola et al., 2015) to analyze SHAPE-MaP results.

Examined structures of spiked-in 5S rRNA in circSHAPE-MaP or linearSHAPE-MaP duplicates were highly correlated (~0.97/0.96, Figure 3C) and comparable to the reported 5S rRNA structure (Figure S5D) (Spitale et al., 2013), confirming that these independent SHAPE-MaP reactions were reliable for circular and linear RNA structure comparison. Secondary structures of circRNAs are different from those of their linear mRNA isoforms. First, two biological replicates of circSHAPE-MaP reactions were highly correlated, suggesting that circRNAs are stable in structure (Figure 3C), whereas linear RNAs appeared to be dynamic and unstable, indicated by the observation that two biological replicates of linearSHAPE-MaP reactions were less correlated (Figure 3C). Second, because examined circRNAs are much shorter in length than their linear cognate RNAs, RNA secondary structures (≥ 16 bp, in length) in circRNAs, exemplified by *circPOLR2A* (Figure 3D), could be detected locally with high probability, while linear RNAs tended to form secondary structures across long distances with relatively low probabilities (Figures 3D, 3E, and S5E). Third, these examined 12 circRNAs tended to form imperfect short RNA duplexes between 16–26 bp (Figures 3F), while such structures were seen less frequently in their linear cognate RNA fragments (Figures 3E and 3F). For instance, two short dsRNAs, 16 bp and 19 bp in length, were found in the 336 nt-long *circPOLR2A*, but neither was detected in the examined linear *POLR2A* with the same sequences (Figures 3D). Three-dimensional modeling based on the circSHAPE-MaP data further illustrated that these two short RNA duplexes were extended toward the outside of *circPOLR2A* (Figure S5F). Such short dsRNAs were also present more frequently in the rest of 11 examined circRNAs than in their linear cognate RNAs (Figure 4A; Table S5). Although we cannot exclude the possibility that protein binding to circRNAs *in vivo* may interfere with the accessibility of NAI probing, this probability also exists for linear RNAs. Thus, this parallel comparison of 12 pairs of circular and their linear cognate RNAs has shown that circRNAs likely exhibit distinct structural conformations from their linear RNAs with the identical sequences.

We also analyzed additional 22 circRNAs that have repeatable circSHAPE-MaP signals but no paired linearSHAPE-MaP data (Figures S5A–S5C). We detected that 14 out of 22 circRNAs formed imperfect dsRNA regions longer than 16 bp; whereas eight circRNAs, such as *circSMARCA5*, did not display detectable dsRNA regions (Figures 4B and 4C; Table 1). Thus, most (76%, 26 out of 34) examined circRNAs likely exhibited short intra-dsRNA regions in cells.

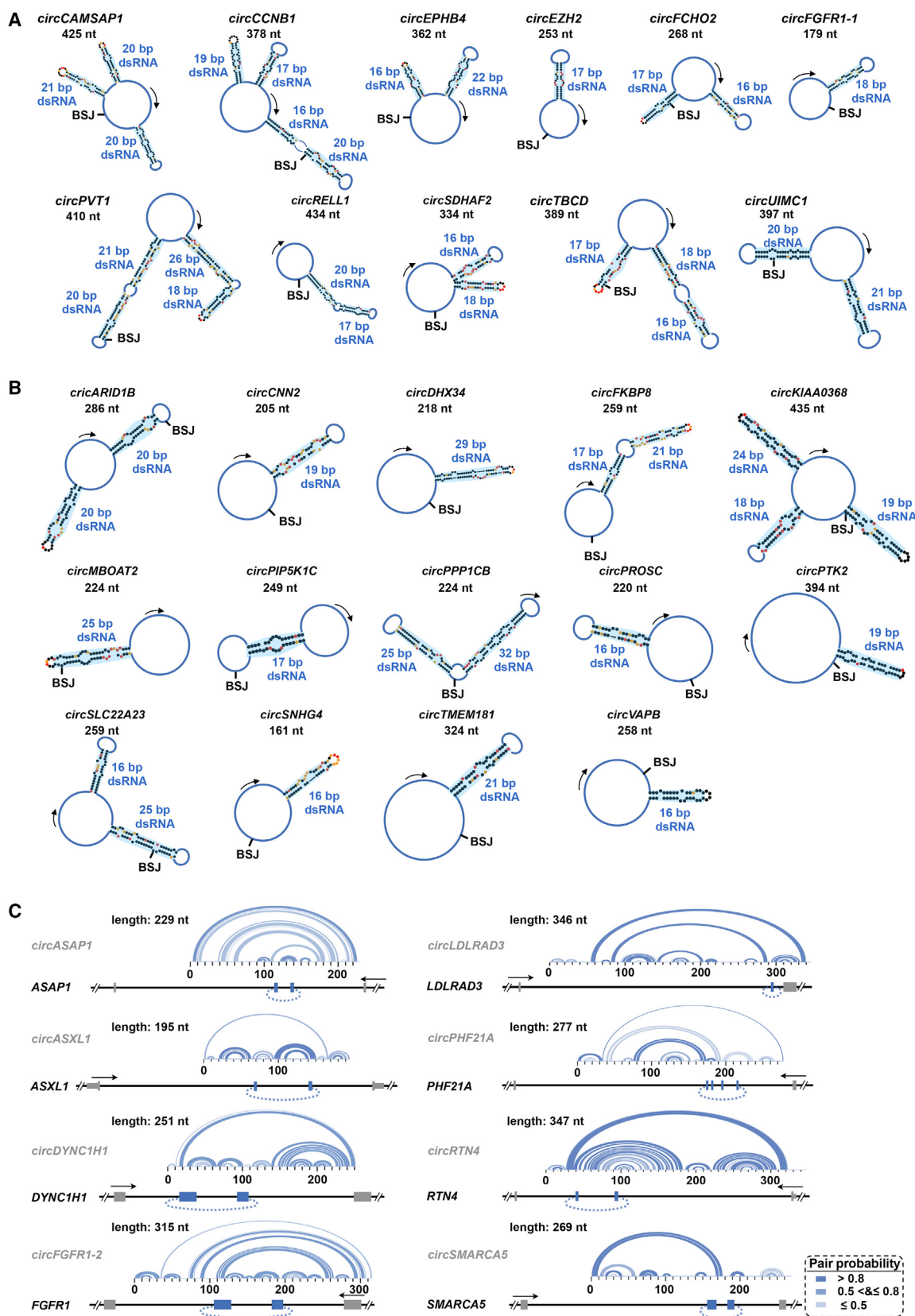
(D) Secondary structure models from in-cell SHAPE reactivities for circular and linear *POLR2A*. Top: *circPOLR2A* contains two imperfect dsRNA modules (blue shadow, 16 bp and 19 bp). Bottom: linear *POLR2A* is relatively unstructured within *circPOLR2A*-forming region (between two blue dashed lines). Potential base pairs are shown as color arcs indicating pair probabilities. *POLR2A* is shown in bottom and *circPOLR2A*-forming exons are indicated in blue.

(E) Pair probabilities of 12 circRNAs are higher than those of linear RNA cognates. Left: each blue dot represents a potential intra-dsRNA (length ≥ 16 bp) region formed in circRNAs (*Circ*), and each black dot represents a potential intra-dsRNA (length ≥ 16 bp) region formed in linear RNAs within circRNA-forming sequence regions (*L_in*). “n” represents the number of 16–26 bp imperfect RNA duplexes potentially formed in *Circ* or *L_in*. Right: illustrations show an imperfect intra-dsRNA region (Heinicke et al., 2011) and “*Circ*” or “*L_in*” in a circRNA or the paired linear RNA. *p < 0.05, F test.

(F) circRNAs form more intra-dsRNA (length ≥ 16 bp) region than their linear cognate RNAs.

(C, E, and F) Data are shown as median and IQR.

See also Figure S5 and Table S5.



(legend on next page)

Endogenous circRNAs Suppress PKR Activation in Cells

We next asked whether such dsRNA-containing circRNAs (Figures 3, 4A, and 4B; Table 1) could regulate PKR activity in cells. As different circRNAs could suppress PKR *in vitro* in a sequence-independent manner (Figures 2H–2J), we hypothesized that circRNAs as a group might associate with PKR in cells to suppress its phosphorylation. Examination of the copy number of *circPOLR2A* in HeLa cells by absolute quantification revealed ~6 copies of *circPOLR2A* per cell (Figure 5A), which was equal to 0.59 FPM (fragments mapped to back-splicing junctions per million mapped fragments) in HeLa cell RNA-seq (Figure 5B). Using FPM values of all detected circRNAs from the RNA-seq (Table S1) as a reference, calculation revealed that per HeLa cell contained ~9,000–10,000 copies of circRNAs under normal condition (Figure 5B). Upon poly(I:C) stimulation for 6 h, circRNAs were reduced to ~1,500 copies per cell (Figure 5B). Considered the fact that most examined circRNAs could form 1–4 dsRNA regions (Table 1), we speculated that per cell contains no less than 10,000–20,000 intra-dsRNA regions and that such circRNAs represent a type of previously under-appreciated endogenous inhibitors for PKR.

To test this model, we examined whether overexpression of circRNAs, such as *circPOLR2A* (Figure 3D) or *circCAMSAP1* (Figure 4A) that contain intra-dsRNA regions, could suppress PKR activation upon poly(I:C) stimulation and whether overexpression of non-dsRNA region containing circRNAs, such as *circSMARCA5* (Figure 4C) would have any effect on PKR activation in the same condition (Figure 5C). The “C” vector for *circ-POLR2A* or the “ndc” vector for *circSMARCA5* produced both circRNA and its linear precursor RNA, while the “L” vector for linear *POLR2A* only produced the linear RNA (Figure 5C). Using these vectors, we found that overexpressed circRNAs yielded ~5,000–6,000 copies per HeLa cell (Figures 5C and S6A).

In WT HeLa cells, PKR activation appeared modestly at 30 min, became much stronger at 60 min, and achieved highly robust activation at 120 min (Figure 5D, WT) upon poly(I:C) exposure. This PKR activation kinetics negatively correlates with the steady-state levels of circRNAs whose half-lives are ~60 min (Figure 1B). In HeLa cells overexpressing C or L vectors (Figure 5C), PKR and its downstream EIF2 α phosphorylation were remarkably reduced by *circPOLR2A* overexpression, compared to little effect by linear *POLR2A* overexpression (Figure 5D) upon poly(I:C) stimulation. Such an inhibitory role of circRNAs was not sequence-dependent, as overexpression of another intra-dsRNA region containing circRNA, *circCAMSAP1*, but not its linear *CAMSAP1* sequences, also led to robust reduction of PKR and EIF2 α phosphorylation (Figure S6A). In contrast, overexpression of *circSMARCA5*, which lacks an intra-dsRNA region (Figure 4C), did not suppress PKR activation upon poly(I:C) treatment (Figure 5E), further supporting

the model that circRNAs suppress PKR activity in cells depending on their intra-molecularly formed dsRNA regions. Similar results were further observed in different time points upon poly(I:C) treatment in both HeLa (Figure 5F, left) and Jurkat (Figure 5F, right) cells. Importantly, this regulation appeared specific to PKR, as circular or linear *POLR2A* overexpression had no measurable effect on TBK1 and IRF3 phosphorylation, which occurs earlier than the PKR activation in response to MAVS (Liu et al., 2015) upon poly(I:C) treatment (Figure 5F).

Consistent with a role of circRNAs in suppression of PKR activation, RNA immunoprecipitation (RIP) with anti-PKR antibodies showed that the endogenous PKR was preferentially associated with examined circRNAs with intra-dsRNA regions in cells (Figure S6B). As a control, no enrichment of *circSMARCA5* could be detected (Figure S6B). Furthermore, full-length Flag-PKR, but not its dsRBM truncation (Figure 2E), was preferentially associated with examined circRNAs with intra-dsRNA regions, but not with *circSMARCA5* that lacks an intra-dsRNA region (Figure 5G). As controls, examined circRNAs exhibited much less binding to Flag-RIG-I using the same anti-Flag antibodies (Figure S6C). In all assays, the full-length Flag-PKR, Flag-tagged PKR dsRBM truncation and Flag-RIG-I were expressed at similar levels (Figures S6D and S6E). Meanwhile, the anti-Flag RIP efficiencies for PKR and its truncation (Figure S6D), as well as PKR and RIG-I (Figure S6E), were comparable.

Collectively, these experiments revealed that circRNAs preferentially bound to PKR to shield its dsRNA-mediated activation. Consistent with this notion, reduced PKR and EIF2 α phosphorylation was observed in RNase L KO cells stimulated with poly(I:C) (Figure 5H). Furthermore, EIF2 α phosphorylation was no longer detected upon poly(I:C) treatment in PKR KO cells, despite of supplementation with additional circular or linear RNAs (Figures S6F and S6G). It is worthwhile noting that poly(I:C) stimulated circRNA degradation was not further increased in PKR KO cells (Figure S6H), excluding the possibility that RNase L-mediated circRNA degradation was due to the competition of exogenous poly(I:C) with circRNAs binding to PKR and subsequently releasing circRNAs for degradation. Moreover, IFN β treatment did not trigger RNase L activation or circRNA degradation (Figure 1A), but it could induce PKR activation via the PACT-mediated signaling pathway (Patel and Sen, 1998). As expected, the addition of circRNAs did not suppress the IFN- β -induced PKR activation (Figure S6I), thus further specifying the model that circRNA degradation by activated RNase L is required for the pathogenic dsRNA-initiated PKR activation, and such regulation is independent of the IFN- β -mediated PKR pathway.

Importantly, overexpression of *circPOLR2A*, but not its linear RNA or *circSMARCA5*, dramatically blocked PKR activation during EMCV infection (Figure 5I), which led to increased EMCV

Figure 4. Many Examined circRNAs Tend to Form Imperfect Duplex RNA Regions

- (A) Secondary structure models of 11 circRNAs from in-cell SHAPE-MaP. Blue shadows show intra-dsRNA regions. BSJ sites and lengths (nt) of circRNAs are labeled. Of note, comparison of all 11 pairs of circRNAs and linear cognates can be accessed in Table S5.
- (B) Secondary structure models of additional 14 circRNAs with intra-dsRNA regions from in-cell SHAPE reactivities.
- (C) circRNAs without detectable intra-dsRNA regions were revealed by in-cell SHAPE reactivities.
- (A–C) Secondary structural models were shown from one of the two SHAPE-MaP replicates.
- (B and C) In-cell SHAPE-MaP assays of their cognate linear RNAs were not performed.
- See also Figure S5 and Table S5.

Table 1. Structural Information of 34 circRNAs by In-Cell SHAPE-MaP

Host Gene of circRNA	circRNA (Chr:Start-End)	Length (nt)	No. of 16–26 bp dsRNAs	Paired Linear RNA SHAPE-MaP
CAMSAP1	chr9:138773478-138774924	425	3	✓
CCNB1	chr5:68470703-68471364	378	4	✓
EPHB4	chr7:100410368-100410830	362	2	✓
EZH2	chr7:148543561-148544397	253	1	✓
FCHO2	chr5:72370568-72373320	268	2	✓
FGFR1-1	chr8:38314873-38315052	179	1	✓
POLR2A	chr17:7402357-7402810	336	2	✓
PVT1	chr8:128902834-128903244	410	4	✓
RELL1	chr4:37633006-37640126	434	2	✓
SDHAF2	chr11:61205096-61205585	334	2	✓
TBCD	chr17:80858526-80869665	389	3	✓
UIMC1	chr5:176370335-176385155	397	2	✓
ARID1B	chr6:157357968-157406039	286	2	NA
CNN2	chr19:1032390-1032695	205	1	NA
DHX34 ^a	chr19:47865732-47865950	218	1 (29 bp)	NA
FKBP8	chr19:18650180-18650530	259	2	NA
KIAA0368	chr9:114148656-114154104	435	3	NP
MBOAT2	chr2:9083315-9098771	224	1	NA
PIP5K1C	chr19:3660963-3661999	249	1	NA
PPP1CB ^b	chr2:29006772-29011675	224	2 (32 bp)	NP
PROSC	chr8:37623043-37623873	220	1	NA
PTK2	chr8:141889569-141900868	394	1	NP
SLC22A23	chr6:3410421-3416089	259	2	NA
SNHG4	chr5:138614015-138614818	161	1	NA
TMEM181	chr6:159004985-159010814	324	1	NA
VAPB	chr20:57014000-57016139	258	1	NA
ASAP1	chr8:131370262-131374017	229	ND	NA
ASXL1	chr20:30954186-30956926	195	ND	NA
DYNC1H1	chr14:102506572-102507010	251	ND	NA
FGFR1-2	chr8:38282026-38283763	315	ND	NA
LDLRAD3	chr11:36248634-36248980	346	ND	NA
PHF21A	chr11:46098304-46113774	277	ND	NA
RTN4	chr2:55209650-55214834	347	ND	NA
SMARCA5	chr4:144464661-144465125	269	ND	NA

The genomic location, length, the number of detected intra-dsRNA regions of each examined circRNA by in-cell SHAPE-MaP are listed. NA, not available; ND, not detected; NP, not passed (filters for analysis).

See also Figure S5 and Table S5.

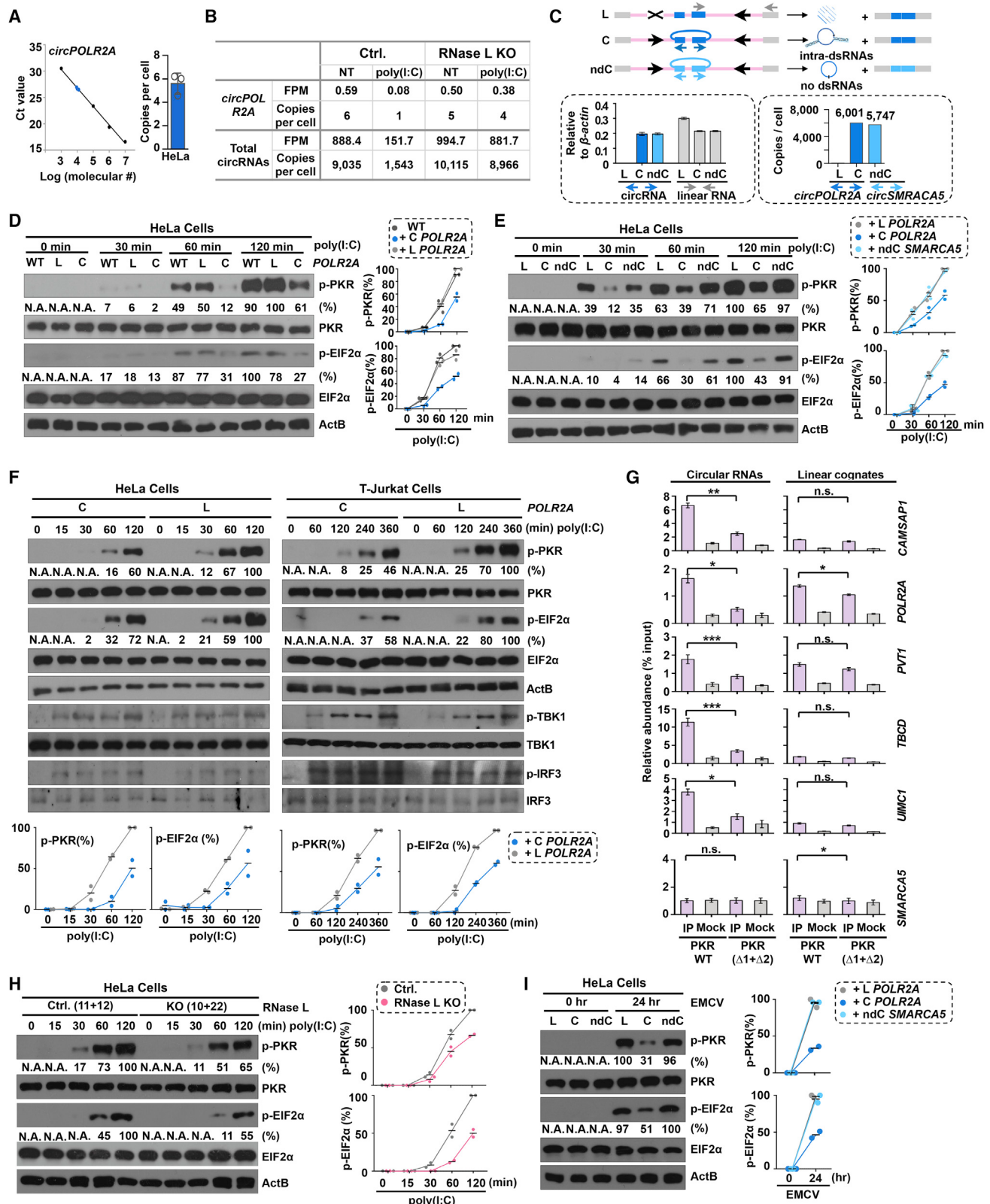
^acircDHX34 has one 29 bp intra-dsRNA region.

^bcircPPP1CB has one 25 bp and one 32 bp intra-dsRNA regions.

mRNA expression in these cells (Figure S6J). Of note, both RNase L and PKR are essential factors in cellular anti-viral responses (Huang et al., 2014; Nallagatla et al., 2011). Consistently, loss of RNase L or PKR resulted in significant cell death upon viral infection (Figure S6K, left) by facilitating viral replication as shown by the increased EMCV mRNA level in cells without RNase L or PKR (Figure S6K, right). Altogether, these findings show that the massive and rapid degradation of circRNAs by RNase L is required for PKR activation in the early stage of the innate immune responses.

Dysregulated circRNA Expression and PKR Activation in SLE

Dysregulation of innate immune response plays a critical role in the development of many autoimmune diseases. SLE, a common and potentially fatal autoimmune disorder, has been characterized by auto-antibody production and a type I IFN signature (Tsokos et al., 2016). An early study indicated that the high expression of PKR is likely associated with SLE (Grolleau et al., 2000). Triggered by this connection, we analyzed the expression of PKR and p-PKR in peripheral blood mononuclear cells



(legend on next page)

(PBMCs) isolated from SLE patients and control normal donors. Remarkably, although only slightly increased PKR expression was observed, we found dramatically increased p-PKR levels (Figures 6A and S7A) in PBMCs isolated from SLE patients compared to those in normal controls.

Further examination of circRNAs having intra-dsRNA duplexes (Figure 3) showed that their expression was reduced in PBMCs from SLE patients compared to those from control normal donors (Figure 6B). As controls, the expression of corresponding linear cognate mRNAs (Figure S7B) was not affected or subtly reduced in SLE (Figures 6B and S7B). Next, we investigated the global expression of circRNAs in SLE and control samples. We collected ribosomal RNA-depleted RNAs from three major mononuclear cell populations including monocytes, B cells, and T cells isolated from PBMCs of pooled SLE patients or normal donors, respectively. All SLE patients were evaluated with clinically recognized IFN scores (Baechler et al., 2003; Feng et al., 2006; Kirov et al., 2004) (Figure S7C; Table S7). RNA-seq analyses revealed a global reduction of both number (Figure 6C) and expression levels (Figure 6D) of circRNAs in all examined cell types derived from SLE patients, compared to those from normal controls. Expression of linear cognate mRNAs (Figure 5E) and all mRNAs (Figure S7D) was also reduced in SLE, but to a less degree compared to circRNAs. Consistently, spontaneous RNase L activation was detected in PBMCs isolated from additional SLE patients but not normal controls (Figure S7E). Compared to the RNase L activation in HeLa cells stimulated with poly(I:C), the observed RNase L activity in SLE was subtle (Figure S7F). Collectively, these analyses suggest a link between RNase L activation, reduced circRNA expression, and augmented PKR activation in SLE.

Finally, we explored whether overexpressing the dsRNA-region containing circRNA could attenuate the aberrant PKR phosphorylation in PBMCs from SLE patients. Assays performed in

PBMCs from three lupus patients have shown that overexpression of *circPOLR2A* rather than its linear RNA fragment (Figure 6F) with the identical sequences led to reduced PKR activation, subtle but measurable EIF2 α phosphorylation (Figure 6G), and suppressed IFN- β and type I IFN-induced genes that represent the well-established molecular gene signature of SLE (Figure 6H). Because PBMCs contain three major mononuclear populations including monocytes, B cells, and T cells, we next asked whether the aberrant PKR activation could be alleviated in an individual cell type. Indeed, similar suppression of PKR activation and its downstream substrates was also achieved by overexpression of circRNAs in T cells isolated from additional SLE-derived PBMCs (Figures 6I and 6J), highlighting the potential of modulating circRNAs to suppress excessive innate immune responses in autoimmune diseases.

DISCUSSION

circRNAs are widely expressed, but the current understanding of their functions is limited. This is in part due to their circular conformation and almost complete sequence-overlap with their linear RNA counterparts, which have made the precise evaluation of circRNA expression and function challenging. Thus, deciphering how circRNAs differ from their linear cognate RNAs is important in appreciating their functional potential.

At the production level, circRNA biogenesis requires spliceosomal machinery and is modulated by both *cis*- and *trans*-factors (for reviews, see Li et al. [2018] and Wilusz [2018]). In contrast, very little is known about their degradation. circRNAs have been thought to be stable because their circular structures are resistant to degradation by linear RNA decay machineries. In this regard, circRNAs can accumulate to relatively high levels in cells that have slow division rates (Rybak-Wolf et al., 2015; Zhang et al., 2016b). Despite of being stable in cells, it remains

Figure 5. circRNAs Prevent PKR Activation in Cells

- (A) Copy number of *circPOLR2A* in HeLa cell. Left: the linear relationship between the log *circPOLR2A* copy number and its CT value by qRT-PCR. Black dots, *circPOLR2A* copy number from the DNA template; blue dots, the examined *circPOLR2A* copy number from 2,000 HeLa cells in triplicates. Right: the average *circPOLR2A* copies per HeLa cell.
- (B) Copy number of total circRNAs in control or RNase L KO HeLa cells upon poly(I:C) stimulation, using FPM values of detected circRNAs in RNA-seq (Tables S1 and S4) and *circPOLR2A* as references.
- (C) Vectors used in the study. Top: vectors used for linear *POLR2A* (L, top), *circPOLR2A* (C, middle), and *circSMARCA5* (non-dsRNA-containing circRNA [ndC], bottom) overexpression in cells. Blue arrows denote divergent primers for circRNA and gray arrows denote convergent primers for *egfp-POLR2A* mRNA detection. Bottom left: circRNA vectors produces both circular and linear RNAs, whereas the L vector only produces linear RNAs shown by qRT-PCR. Bottom right: copy number of each overexpressed circRNA per cell is shown.
- (D) Overexpression of *circPOLR2A*, but not the linear *POLR2A*, in HeLa cells inhibits PKR phosphorylation (p-PKR-T446) upon poly(I:C) stimulation. Cells transfected with individual vectors for 24 h, followed by poly(I:C) treatment at indicated time points. Left: levels of PKR, p-PKR, EIF2 α , p-EIF2 α -S51 (p-EIF2 α for simplicity), and ActB in these cells.
- (E) Overexpression of the non-dsRNA-containing circRNA, *circSMARCA5*, in HeLa cells does not suppress PKR phosphorylation upon poly(I:C) stimulation.
- (F) Overexpression of *circPOLR2A*, but not linear *POLR2A*, in HeLa (left) and Jurkat (right) cells inhibits PKR phosphorylation upon poly(I:C) stimulation. TBK1, p-TBK1-S172 (p-TBK1 for simplicity), IRF3, and p-IRF3-S396 (p-IRF3 for simplicity).
- (G) Flag-PKR is associated with dsRNA-containing circRNAs in cells. HeLa cells stably expressing Flag-PKR or Flag-PKR ($\Delta 1+\Delta 2$) (Figure 2E) were subjected to RIP using anti-Flag (IP) or anti-IgG (Mock) antibodies, respectively. The percentage of RIP-enriched circular and linear cognate RNAs relative to input was revealed under each condition by qRT-PCR. n.s., $p > 0.05$, * $p < 0.05$, ** $p < 0.01$, *** $p < 0.001$, Student's t test.
- (H) Reduced PKR activation in RNase L KO HeLa cells stimulated with poly(I:C).
- (I) Overexpression of *circPOLR2A*, but not the linear cognate *POLR2A* or the non-dsRNA-containing circRNA, *circSMARCA5*, in HeLa cells inhibits PKR phosphorylation upon EMCV infection. HeLa cells were transfected with indicated vectors and then EMCV infection followed by WB.
- (D–F, H, and I) Transfection and WBs were performed twice; the level of p-PKR and p-EIF2 α in each panel was quantified by Quantity One. p-PKR and p-EIF2 α levels were normalized by PKR or EIF2 α expression, respectively. Each dot represents the result from one replicate.
- See also Figure S6.

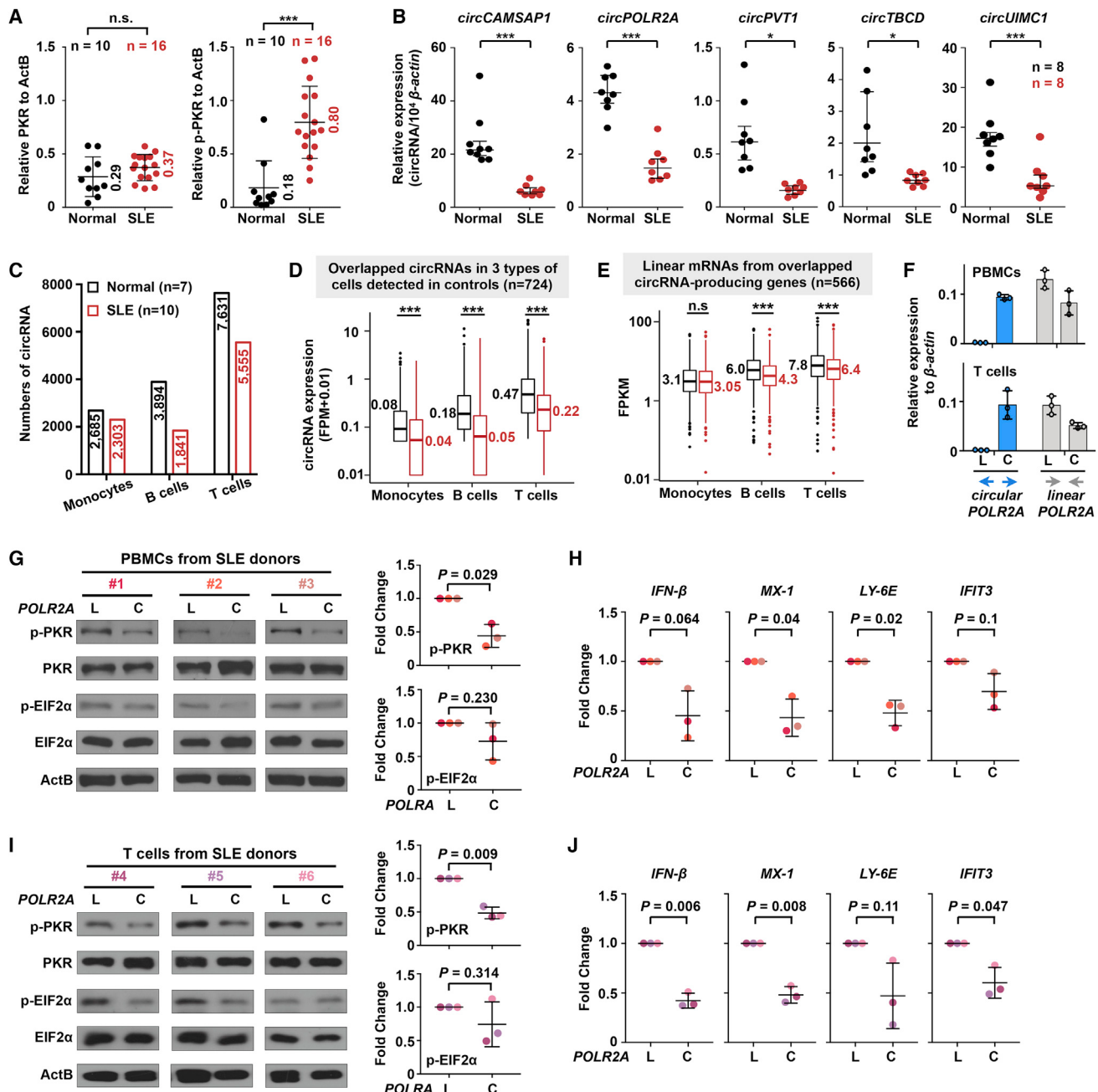


Figure 6. circRNA Reduction and PKR Activation in SLE

- (A) The levels of PKR phosphorylation are higher in PBMCs derived from individual SLE patients (SLE), compared to those in cells isolated from control normal donors.
- (B) Examination of circRNA reduction in PBMCs derived from SLE patients by qRT-PCR.
- (C) Global reduction of circRNA numbers in monocytes, B cells, and T cells derived from SLE patients compared to those in cells derived from normal donors, revealed by RiboMinus RNA-seq.
- (D) Global reduction of circRNA expression in monocytes, B cells, and T cells derived from SLE patients compared to those in cells derived from normal donors, revealed by RNA-seq.
- (E) Subtle reduction of linear cognate mRNA expression in monocytes, B cells, and T cells derived from SLE patients compared to those in cells derived from normal donors, revealed by RNA-seq.
- (F) Expression levels of *circPOLR2A* (C vector) or its linear cognate RNA fragments (L vector) shown in Figure 5C in PBMCs and T cells by transfection.
- (G) *circPOLR2A* overexpression attenuates aberrant PKR and EIF2α phosphorylation in PBMCs isolated from three SLE patients. The level of p-PKR and p-EIF2α in each panel was quantified by Quantity One. p-PKR and p-EIF2α levels were normalized by PKR or EIF2α expression and shown on right.

(legend continued on next page)

possible that unknown endonucleases may initiate cleavage of circRNAs under certain cellular stress. Here, we identify the endonuclease RNase L, once activated, as being able to globally degrade circRNAs (Figures 1 and S2). Intriguingly, although both circRNAs and linear RNAs are degraded by RNase L (Figures 1, S2, and S3), nascent circRNA production is much less efficient than that of nascent linear RNAs (Zhang et al., 2016b). Thus, the amount of nascent circRNAs produced from pre-mRNAs cannot overcome rapid degradation by RNase L within a short period upon early innate immune responses (Figure S3C).

One consequence of circRNA degradation by RNase L upon viral infection is likely to release the circRNA-associated PKR, allowing activation. Although it remains to be explored how exactly circRNAs bind to PKR stoichiometrically, SHAPE-MaP analyses revealed that many (26 out of 34) examined circRNAs tended to form 16–26 bp intra-dsRNA regions (Figures 3 and 4; Table 1). These observations led to the speculation that different RNA circles can act as a group to suppress PKR in a sequence-independent, but structure-dependent manner both *in vitro* (Figures 2H–2J) and in cells (Figures 5D and S6A). Considering that per cell has ~10,000 copies of circRNAs (Figure 5B), and most examined circRNAs could form 1–4 intra-dsRNA regions (Table 1), circRNAs with such intra-dsRNA conformation represent a type of previously unknown inhibitor for PKR in cells. Consistent with this view, circRNA degradation by activated RNase L upon poly(I:C) or virus treatments is required for PKR activation (Figure 5H); the addition of circRNAs having intra-dsRNAs, but not those without such a region or linear cognate RNAs to cells, could alleviate PKR activation in the early stage of innate immune responses (Figures 5A–5F, 5I, and S6A). Of note, we normally observed >5,000 copies of circRNAs (Figure 5C) overexpressed from the plasmids shown in Figure 5C. This yield was enough to significantly increase the overall cellular pool of circRNAs.

Recent evidence suggests that PKR can interact with multiple types of dsRNAs, such as nuclear dsRNAs formed by repeated Alu elements intra-molecularly and mitochondrial dsRNAs (mtdsRNAs) formed by bidirectionally transcribed mitochondrial RNAs inter-molecularly (Kim et al., 2018), consistent with the notion that PKR is an abundant protein (Hein et al., 2015). While nuclear dsRNAs are likely to be retained in the nucleus to restrict cellular dsRNA responses (Chen and Yang, 2017), the level of mtdsRNAs is tightly controlled by degradosome components (Dhir et al., 2018; Borowski et al., 2013). Loss of such enzymes (Dhir et al., 2018) or other cellular stresses (Kim et al., 2018) can result in accumulation of mtdsRNAs that escape into the cytoplasm to engage an MDA5-driven antiviral signaling pathway (Dhir et al., 2018) and the activation of PKR (Kim et al., 2018). Compared to MDA5 and RIG-I, circRNAs were preferentially bound to PKR

(Figures 2A and 2B), probably due to the fact that MDA5 binds to long dsRNAs (Kato et al., 2008), and RIG-I binds to intracellular 5'-triphosphate single-stranded RNA and panhandle-like blunt-end 5'-triphosphate dsRNA (Kowalinski et al., 2011; Pichlmair et al., 2006). Instead, PKR activation requires dsRNAs longer than 33 bp, while short dsRNAs of 16–33 bp in length can block its activation (Zheng and Bevilacqua, 2004; Nallagatla et al., 2011). Because circRNAs are largely distributed in the cytoplasm (Huang et al., 2018), and most examined circRNAs tend to form 16–26 bp RNA duplexes (Table 1), we speculate that circRNAs are naturally existing inhibitors for PKR and possibly other nucleic acid receptors with similar dsRNA binding preferences. Future investigation is warranted to study structures from an even wider spectrum of individual circRNAs and to examine whether such intra-dsRNA structures are prevalent in circRNAs.

Finally, consistent with the role of circRNAs in suppressing PKR activation in normal cultured cells (Figures 1, 2, 3, 4, and 5), SLE patients display reduced circRNA expression, coupled with spontaneous RNase L activation and enhanced PKR activation (Figures 6A–6D and S7). Furthermore, overexpression of circRNAs could robustly alleviate aberrant PKR activation cascade in patient-derived cells (Figures 6F–6J). Although the causality between circRNA expression, RNase L and PKR activation, and SLE still requires further investigation, our findings uncover an unexpected pathophysiological connection of circRNA function to autoimmune diseases.

STAR METHODS

Detailed methods are provided in the online version of this paper and include the following:

- KEY RESOURCES TABLE
- CONTACT FOR REAGENT AND RESOURCE SHARING
- EXPERIMENTAL MODEL AND SUBJECT DETAILS
 - Human cell lines
 - Bacterial strains
 - SLE patients and control normal donors
- METHOD DETAILS
 - Cell culture, transfection and stimulation
 - Plasmid constructions and generation of stable cell lines
 - Lentivirus production and cell infection
 - RNase L or PKR knockout by the CRISPR/Cas9 system
 - RNA isolation, RT-PCR, qRT-PCR
 - Northern blotting (NB)
 - *In vitro* RNA transcription, circularization and purification

(H) *circPOLR2A* overexpression reduces the expression of IFN signature genes in PBMCs isolated from SLE patients, shown by qRT-PCR. Examined IFN- β and IFN signature genes including three representative type I IFN responsive genes for calculating IFN score.

(I) *circPOLR2A* overexpression attenuates aberrant PKR and EIF2 α phosphorylation in T cells isolated from three SLE patients.

(J) *circPOLR2A* overexpression reduces the expression of IFN signature genes in T cells isolated from SLE patients, shown by qRT-PCR. See (H) for details.

(A, B, and G–J) n.s., p > 0.05, *p < 0.05, **p < 0.01, ***p < 0.001, Student's t test, error bars represent SD.

(D and E) n.s., p > 0.05, ***p < 0.001, Wilcoxon rank-sum test. The median, IQR, and 1.5 × IQR are shown.

See also Figure S7 and Tables S6 and S7.

- Protein expression and purification
- Circular/linear RNA binding assay
- Circular/linear RNAs competition assay
- *In vitro* activation assay of PKR
- In-cell SHAPE probing
- SHAPE-MaP reverse transcription
- SHAPE-MaP library preparation and sequencing
- Measurement of circRNA copy number
- RNA Immunoprecipitation (RIP)
- Cell proliferation assay
- Isolation of peripheral blood mononuclear cells (PBMCs) using Ficoll-PaqueTM
- Isolation of monocytes, B cells and T cells from PBMCs
- Plasmid transfection to PBMCs and T cells isolated from SLE patients
- Polyadenylated/non-polyadenylated RNA separation, rRNA depletion for RNA-seq
- Library preparation and deep sequencing
- RtcB-ligase assisted qPCR
- QUANTIFICATION AND STATISTICAL ANALYSIS
 - RNA-seq analyses
 - SHAPE reactivity calculation
 - RNA secondary structure modeling
 - Double-stranded RNA structure analysis
 - Three-dimensional RNA structure modeling
 - Statistical analyses
- DATA AND SOFTWARE AVAILABILITY

SUPPLEMENTAL INFORMATION

Supplemental Information can be found online at <https://doi.org/10.1016/j.cell.2019.03.046>.

ACKNOWLEDGMENTS

We would like to thank G. Carmichael and F. Hou for discussion and Y. Li and X. Zhou for providing EMCV virus. L.-L.C. is supported by the Chinese Academy of Sciences (CAS) (XDB19020104), the Ministry of Science and Technology of China (2016YFA0100701), the National Natural Science Foundation of China (NSFC) (91440202, 31821004, and 31725009), and the Howard Hughes Medical Institute International Program (55008728); L.Y. is supported by NSFC (31730111); N.S. is supported by NSFC (81401331, 31630021); and W.X. is supported by NSFC (31801073), the Youth Innovation Promotion Association CAS, and the Shanghai Sailing Program.

AUTHOR CONTRIBUTIONS

L.-L.C. and L.Y. conceived the project. C.-X.L., X.L., S.J., X.G., and S.-K.G. performed experiments. F.N., W.X., and K.D. preformed computational analyses. Y.C., H.D., B.Q., and N.S. provided SLE and control samples. L.-L.C. and L.Y. wrote the paper with input from C.-X.L., X.L., F.N., and N.S. L.-L.C. supervised the project.

DECLARATION OF INTERESTS

The authors declare no competing interests.

Received: December 13, 2018

Revised: January 29, 2019

Accepted: March 25, 2019

Published: April 25, 2019

REFERENCES

- Baechler, E.C., Battliwalla, F.M., Karypis, G., Gaffney, P.M., Ortmann, W.A., Espe, K.J., Shark, K.B., Grande, W.J., Hughes, K.M., Kapur, V., et al. (2003). Interferon-inducible gene expression signature in peripheral blood cells of patients with severe lupus. *Proc. Natl. Acad. Sci. USA* **100**, 2610–2615.
- Bolger, A.M., Lohse, M., and Usadel, B. (2014). Trimmomatic: a flexible trimmer for Illumina sequence data. *Bioinformatics* **30**, 2114–2120.
- Borowski, L.S., Dziembowski, A., Hejnowicz, M.S., Stepien, P.P., and Szczesny, R.J. (2013). Human mitochondrial RNA decay mediated by PNPase-hSuv3 complex takes place in distinct foci. *Nucleic Acids Res.* **41**, 1223–1240.
- Busan, S., and Weeks, K.M. (2018). Accurate detection of chemical modifications in RNA by mutational profiling (MaP) with ShapeMapper 2. *RNA* **24**, 143–148.
- Chen, L.L., and Yang, L. (2017). ALUternative Regulation for Gene Expression. *Trends Cell Biol.* **27**, 480–490.
- Chen, Y.G., Kim, M.V., Chen, X., Batista, P.J., Aoyama, S., Wilusz, J.E., Iwasaki, A., and Chang, H.Y. (2017). Sensing Self and Foreign Circular RNAs by Intron Identity. *Mol. Cell* **67**, 228–238.
- Deigan, K.E., Li, T.W., Mathews, D.H., and Weeks, K.M. (2009). Accurate SHAPE-directed RNA structure determination. *Proc. Natl. Acad. Sci. USA* **106**, 97–102.
- Dhir, A., Dhir, S., Borowski, L.S., Jimenez, L., Teitel, M., Rötig, A., Crow, Y.J., Rice, G.I., Duffy, D., Tamby, C., et al. (2018). Mitochondrial double-stranded RNA triggers antiviral signalling in humans. *Nature* **560**, 238–242.
- Dong, R., Ma, X.K., Li, G.W., and Yang, L. (2018). CIRCPedia v2: An Updated Database for Comprehensive Circular RNA Annotation and Expression Comparison. *Genomics Proteomics Bioinformatics* **16**, 226–233.
- Donovan, J., Rath, S., Kolet-Mandrikov, D., and Korennykh, A. (2017). Rapid RNase L-driven arrest of protein synthesis in the dsRNA response without degradation of translation machinery. *RNA* **23**, 1660–1671.
- Enuka, Y., Lauriola, M., Feldman, M.E., Sas-Chen, A., Ulitsky, I., and Yarden, Y. (2016). Circular RNAs are long-lived and display only minimal early alterations in response to a growth factor. *Nucleic Acids Res.* **44**, 1370–1383.
- Feng, X., Wu, H., Grossman, J.M., Hanvivadhanakul, P., FitzGerald, J.D., Park, G.S., Dong, X., Chen, W., Kim, M.H., Weng, H.H., et al. (2006). Association of increased interferon-inducible gene expression with disease activity and lupus nephritis in patients with systemic lupus erythematosus. *Arthritis Rheum.* **54**, 2951–2962.
- Groleau, A., Kaplan, M.J., Hanash, S.M., Beretta, L., and Richardson, B. (2000). Impaired translational response and increased protein kinase PKR expression in T cells from lupus patients. *J. Clin. Invest.* **106**, 1561–1568.
- Han, Y., Donovan, J., Rath, S., Whitney, G., Chitrakar, A., and Korennykh, A. (2014). Structure of human RNase L reveals the basis for regulated RNA decay in the IFN response. *Science* **343**, 1244–1248.
- Hein, M.Y., Hubner, N.C., Poser, I., Cox, J., Nagaraj, N., Toyoda, Y., Gak, I.A., Weisswange, I., Mansfeld, J., Buchholz, F., et al. (2015). A human interactome in three quantitative dimensions organized by stoichiometries and abundances. *Cell* **163**, 712–723.
- Heinicke, L.A., Nallagatla, S.R., Hull, C.M., and Bevilacqua, P.C. (2011). RNA helical imperfections regulate activation of the protein kinase PKR: effects of bulge position, size, and geometry. *RNA* **17**, 957–966.
- Hochberg, M.C. (1997). Updating the American College of Rheumatology revised criteria for the classification of systemic lupus erythematosus. *Arthritis Rheum.* **40**, 1725.
- Hofacker, I.L., and Stadler, P.F. (2006). Memory efficient folding algorithms for circular RNA secondary structures. *Bioinformatics* **22**, 1172–1176.
- Huang, H., Zeqiraj, E., Dong, B., Jha, B.K., Duffy, N.M., Orlicky, S., Thevakanmaran, N., Talukdar, M., Pillon, M.C., Ceccarelli, D.F., et al. (2014). Dimeric structure of pseudokinase RNase L bound to 2'-5'A reveals a basis for interferon-induced antiviral activity. *Mol. Cell* **53**, 221–234.

- Huang, C., Liang, D., Tatomer, D.C., and Wilusz, J.E. (2018). A length-dependent evolutionarily conserved pathway controls nuclear export of circular RNAs. *Genes Dev.* 32, 639–644.
- Kato, H., Takeuchi, O., Mikamo-Satoh, E., Hirai, R., Kawai, T., Matsushita, K., Hiiragi, A., Dermody, T.S., Fujita, T., and Akira, S. (2008). Length-dependent recognition of double-stranded ribonucleic acids by retinoic acid-inducible gene-I and melanoma differentiation-associated gene 5. *J. Exp. Med.* 205, 1601–1610.
- Kim, D., and Salzberg, S.L. (2011). TopHat-Fusion: an algorithm for discovery of novel fusion transcripts. *Genome Biol.* 12, R72.
- Kim, D., Langmead, B., and Salzberg, S.L. (2015). HISAT: a fast spliced aligner with low memory requirements. *Nat. Methods* 12, 357–360.
- Kim, Y., Park, J., Kim, S., Kim, M., Kang, M.G., Kwak, C., Kang, M., Kim, B., Rhee, H.W., and Kim, V.N. (2018). PKR Senses Nuclear and Mitochondrial Signals by Interacting with Endogenous Double-Stranded RNAs. *Mol. Cell* 71, 1051–1063.
- Kirou, K.A., Lee, C., George, S., Louca, K., Papagiannis, I.G., Peterson, M.G., Ly, N., Woodward, R.N., Fry, K.E., Lau, A.Y., et al. (2004). Coordinate overexpression of interferon-alpha-induced genes in systemic lupus erythematosus. *Arthritis Rheum.* 50, 3958–3967.
- Kowalinski, E., Lunardi, T., McCarthy, A.A., Louber, J., Brunel, J., Grigorov, B., Gerlier, D., and Cusack, S. (2011). Structural basis for the activation of innate immune pattern-recognition receptor RIG-I by viral RNA. *Cell* 147, 423–435.
- Langmead, B., and Salzberg, S.L. (2012). Fast gapped-read alignment with Bowtie 2. *Nat. Methods* 9, 357–359.
- Langmead, B., Trapnell, C., Pop, M., and Salzberg, S.L. (2009). Ultrafast and memory-efficient alignment of short DNA sequences to the human genome. *Genome Biol.* 10, R25.
- Li, H., Handsaker, B., Wysoker, A., Fennell, T., Ruan, J., Homer, N., Marth, G., Abecasis, G., and Durbin, R.; 1000 Genome Project Data Processing Subgroup (2009). The Sequence Alignment/Map format and SAMtools. *Bioinformatics* 25, 2078–2079.
- Li, X., Liu, C.X., Xue, W., Zhang, Y., Jiang, S., Yin, Q.F., Wei, J., Yao, R.W., Yang, L., and Chen, L.L. (2017). Coordinated circRNA Biogenesis and Function with NF90/NF110 in Viral Infection. *Mol. Cell* 67, 214–227.
- Li, X., Yang, L., and Chen, L.L. (2018). The Biogenesis, Functions, and Challenges of Circular RNAs. *Mol. Cell* 71, 428–442.
- Liu, S., Cai, X., Wu, J., Cong, Q., Chen, X., Li, T., Du, F., Ren, J., Wu, Y.T., Grishin, N.V., and Chen, Z.J. (2015). Phosphorylation of innate immune adaptor proteins MAVS, STING, and TRIF induces IRF3 activation. *Science* 347, aaa2630.
- Lorenz, R., Bernhart, S.H., Höner Zu Siederdissen, C., Tafer, H., Flamm, C., Stadler, P.F., and Hofacker, I.L. (2011). ViennaRNA Package 2.0. Algorithms Mol. Biol. 6, 26.
- Moffat, J., Grueneberg, D.A., Yang, X., Kim, S.Y., Kloepfer, A.M., Hinkle, G., Piqani, B., Eisenhaure, T.M., Luo, B., Grenier, J.K., et al. (2006). A lentiviral RNAi library for human and mouse genes applied to an arrayed viral high-content screen. *Cell* 124, 1283–1298.
- Nallagatla, S.R., Toroney, R., and Bevilacqua, P.C. (2011). Regulation of innate immunity through RNA structure and the protein kinase PKR. *Curr. Opin. Struct. Biol.* 21, 119–127.
- Patel, R.C., and Sen, G.C. (1998). PACT, a protein activator of the interferon-induced protein kinase, PKR. *EMBO J.* 17, 4379–4390.
- Pham, A.M., Santa Maria, F.G., Lahiri, T., Friedman, E., Marié, I.J., and Levy, D.E. (2016). PKR Transduces MDA5-Dependent Signals for Type I IFN Induction. *PLoS Pathog.* 12, e1005489.
- Pichlmair, A., Schulz, O., Tan, C.P., Näslund, T.I., Liljestrom, P., Weber, F., and Reis e Sousa, C. (2006). RIG-I-mediated antiviral responses to single-stranded RNA bearing 5'-phosphates. *Science* 314, 997–1001.
- Rybak-Wolf, A., Stottmeister, C., Glažar, P., Jens, M., Pino, N., Giusti, S., Hanan, M., Behm, M., Bartok, O., Ashwal-Fluss, R., et al. (2015). Circular RNAs in the Mammalian Brain Are Highly Abundant, Conserved, and Dynamically Expressed. *Mol. Cell* 58, 870–885.
- Schlee, M., and Hartmann, G. (2016). Discriminating self from non-self in nucleic acid sensing. *Nat. Rev. Immunol.* 16, 566–580.
- Smola, M.J., Rice, G.M., Busan, S., Siegfried, N.A., and Weeks, K.M. (2015). Selective 2'-hydroxyl acylation analyzed by primer extension and mutational profiling (SHAPE-MaP) for direct, versatile and accurate RNA structure analysis. *Nat. Protoc.* 10, 1643–1669.
- Spitale, R.C., Crisalli, P., Flynn, R.A., Torre, E.A., Kool, E.T., and Chang, H.Y. (2013). RNA SHAPE analysis in living cells. *Nat. Chem. Biol.* 9, 18–20.
- Taylor, S.S., Haste, N.M., and Ghosh, G. (2005). PKR and eIF2alpha: integration of kinase dimerization, activation, and substrate docking. *Cell* 122, 823–825.
- Trapnell, C., Williams, B.A., Pertea, G., Mortazavi, A., Kwan, G., van Baren, M.J., Salzberg, S.L., Wold, B.J., and Pachter, L. (2010). Transcript assembly and quantification by RNA-Seq reveals unannotated transcripts and isoform switching during cell differentiation. *Nat. Biotechnol.* 28, 511–515.
- Tsokos, G.C., Lo, M.S., Costa Reis, P., and Sullivan, K.E. (2016). New insights into the immunopathogenesis of systemic lupus erythematosus. *Nat. Rev. Rheumatol.* 12, 716–730.
- Wang, L., Wang, S., and Li, W. (2012). RSeQC: quality control of RNA-seq experiments. *Bioinformatics* 28, 2184–2185.
- Wang, J., Mao, K., Zhao, Y., Zeng, C., Xiang, J., Zhang, Y., and Xiao, Y. (2017). Optimization of RNA 3D structure prediction using evolutionary restraints of nucleotide-nucleotide interactions from direct coupling analysis. *Nucleic Acids Res.* 45, 6299–6309.
- Wilusz, J.E. (2018). A 360° view of circular RNAs: From biogenesis to functions. *Wiley Interdiscip. Rev. RNA* 9, e1478.
- Wu, Y., Liang, D., Wang, Y., Bai, M., Tang, W., Bao, S., Yan, Z., Li, D., and Li, J. (2013). Correction of a genetic disease in mouse via use of CRISPR-Cas9. *Cell Stem Cell* 13, 659–662.
- Yan, J., Xiang, J., Lin, Y., Ma, J., Zhang, J., Zhang, H., Sun, J., Danial, N.N., Liu, J., and Lin, A. (2013). Inactivation of BAD by IKK inhibits TNF α -induced apoptosis independently of NF- κ B activation. *Cell* 152, 304–315.
- Yang, L., Duff, M.O., Graveley, B.R., Carmichael, G.G., and Chen, L.L. (2011). Genomewide characterization of non-polyadenylated RNAs. *Genome Biol.* 12, R16.
- Yin, Q.F., Chen, L.L., and Yang, L. (2015). Fractionation of non-polyadenylated and ribosomal-free RNAs from mammalian cells. *Methods Mol. Biol.* 1206, 69–80.
- Zhang, X.O., Wang, H.B., Zhang, Y., Lu, X., Chen, L.L., and Yang, L. (2014). Complementary sequence-mediated exon circularization. *Cell* 159, 134–147.
- Zhang, X.O., Dong, R., Zhang, Y., Zhang, J.L., Luo, Z., Zhang, J., Chen, L.L., and Yang, L. (2016a). Diverse alternative back-splicing and alternative splicing landscape of circular RNAs. *Genome Res.* 26, 1277–1287.
- Zhang, Y., Xue, W., Li, X., Zhang, J., Chen, S., Zhang, J.L., Yang, L., and Chen, L.L. (2016b). The Biogenesis of Nascent Circular RNAs. *Cell Rep.* 15, 611–624.
- Zhang, S.Y., Clark, N.E., Freije, C.A., Pauwels, E., Taggart, A.J., Okada, S., Mandel, H., Garcia, P., Ciancanelli, M.J., Biran, A., et al. (2018). Inborn Errors of RNA Lariat Metabolism in Humans with Brainstem Viral Infection. *Cell* 172, 952–965.
- Zhao, Y., Huang, Y., Gong, Z., Wang, Y., Man, J., and Xiao, Y. (2012). Automated and fast building of three-dimensional RNA structures. *Sci. Rep.* 2, 734.
- Zheng, X., and Bevilacqua, P.C. (2004). Activation of the protein kinase PKR by short double-stranded RNAs with single-stranded tails. *RNA* 10, 1934–1945.

STAR★METHODS

KEY RESOURCES TABLE

REAGENT or RESOURCE	SOURCE	IDENTIFIER
Antibodies		
Anti-RNase L	Abcam	Cat# ab191392
Anti-β-Actin	Sigma	Cat# A3854; RRID: AB_262011
Anti-FLAG	Sigma	Cat# F1804; RRID: AB_262044
Anti-PKR	Abways	Cat# CY5665
Anti-Phospho-PKR (T446)	Abways	Cat# CY5271
Anti-TBK1	CST	Cat# 3504; RRID: AB_2255663
Anti-Phospho-TBK1 (Ser172)	CST	Cat# 5483; RRID: AB_10693472
Anti-IRF-3	CST	Cat# 4302; RRID: AB_1904036
Anti-Phospho-IRF-3 (Ser396)	CST	Cat# 4947; RRID: AB_823547
Anti-eIF2α	ABclonal	Cat# A0764; RRID: AB_10686196
Anti-Phospho-eIF2α (S51)	ABclonal	Cat# AP0342
Anti-rabbit-IgG-HRP	Santa Cruz	Cat# sc-2004; RRID: AB_631746
Anti-mouse-IgG-HRP	Santa Cruz	Cat# sc-2005; RRID: AB_631736
Bacterial and Virus Strains		
Encephalomyocarditis virus (EMCV)	Fudan University	ATCC VR 129B
BL21	Transgen	Cat# CD801
Biological Samples		
Monocytes, B cells, T cells or peripheral blood mononuclear cells (PBMCs) derived from SLE patients and control normal donors	Renji Hospital, Shanghai	https://www.renji.com/
Chemicals, Peptides, and Recombinant Proteins		
Poly(I:C)	Sigma	Cat# P9582
lipopolysaccharide (LPS)	ABCONE	Cat# L26331
thapsigargin (Tg)	Sigma	Cat# T9033
IFNβ	PEPROTECH	Cat# 300-02BC
IFNγ	PEPROTECH	Cat# 300-02
α-Amanitin	Sigma	Cat# A2263
2-5A	ChemGenes	N/A
RtcB Ligase	NEB	Cat# MO458S
doxycycline (Dox)	Clontech	Cat# 631311
T4 Polynucleotide Kinase	NEB	Cat# M0201
RNase R	Epicenter	Cat# MRNA092
T4 RNA Ligase I	NEB	Cat# M0204L
cComplete ULTRA Tablets, Mini, EASYpack Protease Inhibitor Cocktail	Roche	Cat# 000000005892970001
Ribonucleoside Vanadyl Complex	NEB	Cat# S1402S
Dynabeads Protein G	Invitrogen	Cat# 1003D
CD3 MicroBeads human	Miltenyi	Cat# 130-050-101
CD14 MicroBeads, human	Miltenyi	Cat# 130-050-201
CD19 MicroBeads human	Miltenyi	Cat# 130-050-301
Lipofectamine 2000 Reagent	Thermo	Cat# 11668019
X-tremeGENE 9	Roche	Cat# 6366236001
Hoechst 33342	Sigma	Cat# B2261-25MG

(Continued on next page)

Continued

REAGENT or RESOURCE	SOURCE	IDENTIFIER
Glutathione Sepharose 4B	GE healthcare	Cat# 17-0756-01
DMEM	GIBCO	Cat# 11965
FBS	GIBCO	Cat# 10438-026
TRIzol Reagent	Ambion	Cat# 15596018
DPBS	GIBCO	Cat# 14190-135
Glycerol	ABCONE	Cat# G46055
HEPES	ABCONE	Cat# H33755
TWEEN 20	ABCONE	Cat# P87875
Triton X-100	ABCONE	Cat# X10010
Agarose	ABCONE	Cat# A47902
Bovine Serum Albumin	ABCONE	Cat# A23088
2-methylnicotinic acid imidazolidine (NAI)	EMD Millipore	Cat# 03-310
Critical Commercial Assays		
DNA-free kit	Ambion	Cat# AM1907
DIG Northern Starter Kit	Roche	Cat# 12039672910
Mut Express MultiS Fast Mutagenesis Kit	Vazyme	Cat# C213-01
Hieff Clone One Step Cloning Kit	Yeasen	Cat# 10905ES25
2 × T5 Super PCR Mix	TSINGKE	Cat# TSE005
Phanta Max Super-Fidelity DNA Polymerase	Vazyme	Cat# P505
SuperScript III Reverse Transcriptase	Invitrogen	Cat# 18080044
SuperScript II Reverse Transcriptase	Invitrogen	Cat# 18064071
Hifair III One step RT-qPCR Probe Kit	Yeasen	Cat# 11145
RiboMAX Large Scale RNA Production System	Promega	Cat# P1300
StarPrep Gel Extraction Kit StarPrep	GenStar	Cat# D205-04
Q5 High-Fidelity 2X Master Mix	NEB	Cat# M0492
CellTiter 96 AQueous One Solution Cell Proliferation Assay	Promega	Cat# G3582
Deposited Data		
Linear and circular RNA expression in HeLa cells under different conditions	This paper	NODE: OEP00216; GEO: GSE122967
SHAPE-Map data of linear and circular RNAs	This paper	GEO: GSE126195
Linear and circular RNA expression in normal and SLE donors	This paper	NODE: OEP000216
Original unprocessed data were uploaded to Mendeley Data	This paper	https://doi.org/10.17632/bs6fz5m5th.1
Experimental Models: Cell Lines		
PA1	ATCC	Cat#CRL-1572
HeLa	ATCC	Cat#CCL-2
293FT	Thermo Fisher	Cat# R70007
Jurkat	ATCC	Cat#TIB-152
THP1	ATCC	Cat#TIB-202
Oligonucleotides		
shRNA target sequences: RNase L	This paper	N/A
shRNA1:GGCATCGTGATTCCATATGT		
shRNA target sequences: RNase L	This paper	N/A
shRNA2:GTGGACGACTAAGATTAATGA		
sgRNA target sequences: RNase L	This paper	N/A
sgRNA:TTATCCTCGCAGCGATTGCG		

(Continued on next page)

Continued

REAGENT or RESOURCE	SOURCE	IDENTIFIER
sgRNA target sequences: PKR	This paper	N/A
sgRNA:CCACATGATAGGAGGTAGGTTGC		
Other primers and shRNA target sequences, see Table S5	This paper	N/A
Recombinant DNA		
P23-Flag-RNase L (WT)	This paper	N/A
P23-Flag-RNase L (H672N)	This paper	N/A
pLKO.1-TRC vector	Moffat et al., 2006	Addgene Plasmid # 10878
px330 vector	Wu et al., 2013	Addgene Plasmid # 98750
P23-Flag-PKR	This paper	N/A
P23-Flag-PKR ($\Delta 1+\Delta 2$)	This paper	N/A
P23-Flag-RIG-I	This paper	N/A
pET-28a-His-RIG-1	This paper	N/A
pET-28a-His-TLR3	This paper	N/A
pET-28a-His-MDA5	This paper	N/A
pET-28a-His-PKR	This paper	N/A
pET-28a-His-PKR ($\Delta 1+\Delta 2$)	This paper	N/A
pET-28a-His-NF90	This paper	N/A
pET-28a-His-ADAR1-p150	This paper	N/A
pET-28a-His-OAS1	This paper	N/A
pZW1-circPOLR2A	Zhang et al., 2014	Addgene Plasmid # 73449
pZW1-circPOLR2A-mut	Zhang et al., 2014	N/A
Software and Algorithms		
GraphPad Prism	GraphPad Software	http://www.graphpad.com/scientificsoftware/prism/
Trimmomatic-0.32	Bolger et al., 2014	http://www.usadellab.org/cms/?page=trimmomatic
Bowtie 0.12.9	Langmead et al., 2009	http://bowtie-bio.sourceforge.net/index.shtml
HISAT2 2.0.5	Kim et al., 2015	https://ccb.jhu.edu/software/hisat2/index.shtml
RSeQC 2.6.4	Wang et al., 2012	http://rseqc.sourceforge.net/
TopHat-Fusion v2.0.12	Kim and Salzberg, 2011	http://ccb.jhu.edu/software/tophat/fusion_index.shtml
CIRCExplorer 1.1.10	Zhang et al., 2014	https://github.com/YangLab/CIRCExplorer
Samtools Version: 0.1.18	Li et al., 2009	http://samtools.sourceforge.net/
ShapeMapper 2.1.3	Busan and Weeks, 2018	https://github.com/Weeks-UNC/shapemapper2
Bowtie v2.1.0	Langmead and Salzberg, 2012	http://bowtie-bio.sourceforge.net/bowtie2/index.shtml
CIRCshapemapper	This paper	https://github.com/YangLab/CIRCshapemapper
RNAfold v2.4.2	Lorenz et al., 2011	https://www.tbi.univie.ac.at/RNA/
3dRNA v2.0	Zhao et al., 2012	http://biophy.hust.edu.cn/3dRNA/
R v.3.5.1	https://www.r-project.org	https://www.r-project.org
FPKM	Trapnell et al., 2010	N/A
FPM	Dong et al., 2018	N/A

CONTACT FOR REAGENT AND RESOURCE SHARING

Further information and requests for reagents may be directed to, and will be fulfilled by, the Lead Contact, Ling-Ling Chen (linglingchen@sibcb.ac.cn).

EXPERIMENTAL MODEL AND SUBJECT DETAILS

Human cell lines

Human cell lines including HeLa, PA1, Jurkat and THP1 cells were purchased from the American Type Culture Collection (ATCC; <http://www.atcc.org>) and 293FT purchased from ThermoFisher, and were originally authenticated using STR profiling. HeLa cells (human female origin) and 293FT cells (human fetus origin) were maintained in DMEM supplemented with 10% Fetal Bovine Serum (FBS) and 0.1% penicillin/streptomycin. PA1 cells (human female origin) were maintained in MEM α supplemented with 10% FBS, 1% Glutamine and 0.1% penicillin/streptomycin. Jurkat (human male origin) and THP1 (human male origin) cells were cultured in RPMI supplemented with 10% Fetal Bovine Serum (FBS) and 0.1% penicillin/streptomycin. We maintained cell lines at 37°C in a 5% CO₂ cell culture incubator and tested all cell lines routinely for Mycoplasma contamination.

Bacterial strains

E.coli expression strain BL21 [Tranetta (DE3) chemically competent cell] were procured from Transgen Biotech (Cat# CD801) and were grown in LB culture at 37°C.

SLE patients and control normal donors

All SLE patients (age ranging from 16 to 50, female, [Table S7](#)) were recruited from Renji Hospital, Shanghai Jiao Tong University School of Medicine. All patients fulfilled the 1997 American College of Rheumatology (ACR) classification criteria for SLE ([Hochberg, 1997](#)). All patients were admitted to the department of rheumatology and control normal donors were recruited the department of rheumatology. The study was approved by the Research Ethics Board of Renji Hospital, Shanghai Jiao Tong University School of Medicine. Written informed consent was signed before sample collection.

METHOD DETAILS

Cell culture, transfection and stimulation

Human cell lines including HeLa, 293FT, PA1 and THP1 were maintained using standard protocols from ATCC. Plasmid or poly(I:C) transfection was carried out using X-treme GENE 9 (Roche) or Lipofectamine 2000 Reagent (Thermo) for HeLa and PA1 cells according to the manufacturer's protocols. About 70%–80% transfection efficiency was achieved in HeLa and PA1 cells. Plasmid transfection for THP1, Jurkat cells, SLE patients-derived PBMC and T cells was carried out using electroporation by Neon Transfection System (Invitrogen), with about 40% transfection efficiency in general. For the treatments of different stimulators, poly(I:C) (1 μg/mL, Sigma, catalog #P9582), HT-DNA (5 μg/mL) and ISD (5 μg/mL) was individually transfected into cells for 6 hours (or other indicated time); LPS (300 ng/mL), Tg (3 μM), IFN β (2,000 U/mL), IFN γ (2,000 U/mL) and α -amanitin (2 μg/mL) were directly added into culture medium for 6 hours, and EMCV (0.1 moi) was directly added into culture medium of HeLa cells for 24 hours, then protein or total RNAs were collected for further analyses.

Plasmid constructions and generation of stable cell lines

For RNase L knockdown, DNA sequences for shRNAs that target RNase L mRNA or for a scramble shRNA were individually cloned into pLKO.1-TRC vector. HeLa cells were infected by lentiviral shRNAs to generate stable cell lines with RNase L knockdown. To overexpress RNase L, RIGI or PKR, the N-terminal FLAG-fused RNase L, RIGI or PKR DNA sequences were amplified by Phanta Super-Fidelity DNA Polymerase (Vazyme Biotech) from HeLa cells and cloned into the p23-phage vector. The plasmids were stably transfected into HeLa cells. To overexpress Flag-tagged RNase L nuclease-dead mutation (H672N), the N-terminal FLAG-fused RNase L nuclease-dead mutation (H672N) DNA sequence was created from the N-terminal FLAG-fused RNase L using the QuikChange Site-Directed Mutagenesis Kit (Stratagene). To generate plasmids for protein expression and purification, target DNA sequences, including RIGI, MAD5, TLR3, PKR, NF90, OAS1, ADAR1-p150, STAU1, STAU2, DDX5 and DDX21, were amplified by Phanta Super-Fidelity DNA Polymerase (Vazyme Biotech) from HeLa cells and cloned into pET-28a vector. PKR or NF90 with its dsRBMs deletion was created from the WT PKR or NF90 respectively using the QuikChange Site-Directed Mutagenesis Kit (Stratagene).

Primers for plasmid constructions were listed in [Table S5](#). All constructs were confirmed by Sanger sequencing.

Lentivirus production and cell infection

To produce lentiviral particles, 5×10^6 293FT cells in a 10-cm dish were co-transfected with 10 μg pLKO.1 shRNA construct, 7.5 μg of psPAX2 and 3 μg pMD2.G. The supernatant containing viral particles was harvested twice at 48 and 72 hr after transfection, and filtered through Millex-GP Filter Unit (0.22 μm pore size, Millipore). Viral particles were then concentrated about 100-fold by sucrose gradient ultracentrifugation, resuspended in PBS containing 0.1% BSA, and stored at –80°C until use. To infect HeLa cells with lentivirus, cells were incubated with culture medium containing 10 μL concentrated lentivirus and 5 μg/mL polybrene (Sigma) at 37°C for 1 hr. To increase knockdown efficiency, infected cells were under several days of puromycin selection. Knockdown efficiency of proteins was evaluated by WB. ActB was used as internal control.

RNase L or PKR knockout by the CRISPR/Cas9 system

Sequences for sgRNAs that target RNase L or PKR were inserted into PX330 plasmid (Addgene) that contains sequence encoding Cas9. HeLa cells were transfected with this plasmid by Lipofectamine 2000 Reagent (Thermo) according to the manufacturer's instructions. Protein of selected single clones was extracted for knockout efficiency validation by WB. Finally, two single clones with RNase L knockout (KO) and three single clones with PKR KO were selected and mixed together respectively for further analyses, and two single clones without RNase L or PKR KO were mixed and used as control. RNase L or PKR KO was validated by western blotting (WB). ActB was used as an internal control.

RNA isolation, RT-PCR, qRT-PCR

Total RNAs from cultured cells were extracted with Trizol (Life technologies) according to the manufacturer's protocol. RNAs were treated with DNase I (Ambion, DNA-freeTM kit). cDNAs were reverse transcribed with SuperScript III (Invitrogen) and applied for PCR/qPCR analysis. β-actin mRNA or 18S rRNA were examined as an internal control for normalization. Expression of each examined gene was determined from three independent experiments. Primers for RT-PCR and qRT-PCR were listed in [Table S5](#).

Northern blotting (NB)

NB was performed according to the manufacturer's protocol (DIG Northern Starter Kit, Roche). Digoxigenin (Dig)-labeled antisense riboprobes were made using RiboMAX Large Scale RNA Production Systems (Promega). In brief, 5 µg total RNAs or 1 ng *in vitro* synthesized linear or circular RNAs was resolved on denaturing urea polyacrylamide gel, transferred to nylon membrane (Roche) and UV-crosslinked using standard manufacturer's protocol. Membrane was then hybridized with specific Dig-labeled riboRNA probes. NB probes were listed in [Table S5](#).

In vitro RNA transcription, circularization and purification

Linear RNAs were *in vitro* transcribed from T7 expression vector prepared by RiboMax large RNA production system (Promega) according to the manufacturer's protocol with slight modifications. Briefly, 1 µg PCR-amplified T7-DNA fragments were incubated with 2 µL T7 RNA polymerase enzyme and 0.5 mM dNTPs. 2 mM GMP was supplemented in the reaction to produce 5'-monophosphate RNA that is required for subsequent RNA circularization. *In vitro* transcription was carried out for 2 hr at 37°C, followed by DNase I treatment for 30 min at 37°C to remove DNA templates. Transcribed RNAs were precipitated with ethanol and washed with 75% ethanol and resuspended in RNase-free water.

For *in vitro* circularization, 50 µg linear RNAs were incubated with T4 RNA ligase 1 (NEB) in 500 µL reaction for overnight at 16°C according to the manufacturer's protocol. Circularized or linear RNAs were then concentrated by ethanol precipitation, resolved on denaturing urea polyacrylamide gel and visualized by Ethidium bromide staining. Corresponding bands on denaturing urea polyacrylamide gel were excised for circular or linear RNA purification. Purified circular or linear RNAs were validated by RNase R treatment as described ([Zhang et al., 2014](#)). Primers for circularization were listed in [Table S5](#).

Protein expression and purification

Expression plasmids (with pET-28a as backbone vector) for His-tagged proteins were individually transformed into E.coli expression strain BL21 [Transetta (DE3) chemically competent cell (Transgen Biotech, CD801)]. 5 mL LB culture supplemented with 100 µg/L kanamycin was incubated with a single colony at 250 rpm, 37°C. After overnight growth, the culture was diluted 100-fold into 100 mL LB culture supplemented with 100 µg/L kanamycin. Absorbance was monitored at a wavelength of 600 nm, and upon reaching an optical density (OD600) of 0.4, protein expression was induced by adding of 1 mM IPTG. After overnight incubation at 250 rpm, 16°C, cell pellets were harvested by centrifugation (5,000 rpm, 10 min, 4°C). Cell pellets were resuspended in lysis buffer (50 mM Tris pH 8.0, 300 mM NaCl, 20 mM imidazole, 1 mM PMSF) supplemented with 1 mg/mL lysozyme, and stored on ice for 30 min, followed by 10 min (5 s on/off) sonication on ice. After centrifugation at 10,000 rpm for 30 min at 4°C, the supernatant cell lysates were incubated with Ni Sepharose (GE healthcare) for 2 hr at 4°C. The Sepharose was washed 4 times with washing buffer (50 mM Tris pH 8.0, 300 mM NaCl, 40 mM imidazole, 1 mM PMSF), and bound protein was eluted with elution buffer (50 mM Tris pH 8.0, 300 mM NaCl, 300 mM imidazole). Elution was repeated twice to gain maximum yield. The concentration of purified protein was determined by using Modified Bradford Protein Assay Kit (Sangon Biotech, C503041) and checked by SDS-PAGE.

Circular/linear RNA binding assay

In vitro synthesized linear or circular RNAs were heated for 5 min at 65°C in RNA-folding buffer (10 mM HEPES and 10 mM MgCl₂) and slowly cooled down to room temperature. Equal amounts (1 µg) of folded linear or circular RNAs were added to incubate with 1 µg His-tagged proteins for 2 hr at 4°C in 0.2 mL Binding buffer (50 mM HEPES at pH 7.0, 150 mM NaCl, 10 mM MgCl₂, 0.1 mM DTT, 0.5 mM PMSF, 2mM RVC). Associated linear or circular RNAs with His-tagged proteins were collected by anti-His antibodies and extracted with Trizol (Life technologies) according to the manufacturer's protocol. The relative abundance of circular or linear RNAs that bound to individual His-tagged proteins was assayed by NB using specific Dig-labeled probes.

Circular/linear RNAs competition assay

In vitro synthesized linear and circular RNAs were heated for 5 min at 65°C in RNA-folding buffer (10 mM HEPES and 10 mM MgCl₂) and slowly cooled down to room temperature. Equal amounts of folded linear (0.5 µg) and circular (0.5 µg) RNAs were added to incubate with 1 µg His-tagged proteins for 2 hr at 4°C in 0.2 mL Binding buffer (50 mM HEPES at pH 7.0, 150 mM NaCl, 10 mM MgCl₂, 0.1 mM DTT, 0.5 mM PMSF, 2mM RVC). Associated linear and circular RNAs with His-tagged proteins were collected by anti-His antibodies and extracted with Trizol (Life technologies) according to the manufacturer's protocol. The relative abundance of circular or linear RNAs that bound to different His-tagged proteins was assayed by NB using specific Dig-labeled probes.

In vitro activation assay of PKR

In vitro activation assay of PKR was performed as previously described (Yan et al., 2013) with modifications. Briefly, HeLa cell extracts with overexpressed Flag-tagged PKR were prepared with WCE buffer (20 mM HEPES at pH 7.4, 75 mM NaCl, 2.5 mM MgCl₂, 0.1 mM EDTA, 0.05% Triton X-100, 0.5 mM DTT, 20 mM β-glycerolphosphate, 0.1 mM Na₃VO₄, 2g/mL of leupeptin, and 100 pg/mL of PMSF). Cellular crude lysates were centrifuged at 12,000 rpm for 15 min at 4°C and the supernatants were pre-cleaned with 15 mL Dynabeads Protein G (Invitrogen) to remove non-specific binding. Then, pre-cleaned lysates were used for IP with anti-Flag antibodies (Sigma). IPs were carried out for 2 hr at 4°C. The beads were washed 4 times in HEPES binding buffer (20 mM HEPES at pH 7.7, 50 mM NaCl, 2.5 mM MgCl₂, 0.1 mM EDTA, 0.05% Triton X-100), the pelleted beads were resuspended in kinase buffer (20 mM HEPES at pH 7.6, 20 mM MgCl₂, 20 mM β-glycerolphosphate, 20 mM p-nitrophenyl phosphate, 0.1 mM Na₃VO₄, 2 mM DTT) containing 50 µM ATP. After 20 min at 30°C the reaction was terminated by washing with HEPES binding buffer. Phosphorylated proteins were eluted with 30 µL 1x SDS loading buffer and resolved on 10% SDS-polyacrylamide gel, followed by WBs with antibodies (Abways) against PKR or phospho-PKR (p-PKR, T446).

In-cell SHAPE probing

In-cell SHAPE probing was performed in PA1 cells as previously described (Smola et al., 2015) with modifications. Briefly, PA1 cells were cultured on 10-cm dishes for two days to reach 5 × 10⁶ cells. After washed with PBS, PA1 cells were incubated with 900 µL of fresh cell culture medium and 100 µL of 10x SHAPE Chemical in DMSO with the final concentration of NAI (EMD Millipore) at 100 mM for 10 minutes at 37°C. After removed probing medium, RNAs were isolated by 1 mL Trizol reagent (Invitrogen) according to the manufacturer's protocol. The same procedure was also performed for untreated control samples, but with the addition of only DMSO. In the denaturing control (DC) reaction, RNA was suspended in a denaturing buffer containing formamide and was incubated at 95°C before modification with SHAPE reagents.

SHAPE-MaP reverse transcription

Isolated RNAs were treated with DNase I (Ambion, DNA-free™ kit) to remove possible DNA contamination. About 50-100 ng of RNAs were obtained under each treatment, and were then used for SHAPE-MaP reverse transcription by adding 1 µL (200 U/µL) of SuperScript II (Invitrogen), 6 mM Mn²⁺ and gene-specific primers for linear or circular RNAs (5S rRNA was used as a spike-in control). All primers were listed in Table S5. Mn²⁺ was removed using G-25 micro-spin columns (GE Healthcare) after SHAPE-MaP reverse transcription. Second-strand synthesis was performed with Q5 hot start high-fidelity DNA polymerase and nested PCR was performed to further improve DNA yield. The resulting PCR products were further isolated with PureLink micr spin columns (Life Technologies). Primers for SHAPE-MaP reverse transcription and second-strand synthesis (1st round PCR and nested PCR reactions) were listed in Table S5.

SHAPE-MaP library preparation and sequencing

SHAPE-MaP libraries were prepared from 1 ng of DNAs for linear (linearSHAPE-MaP) or circular (circSHAPE-MaP) RNAs, and size-selected with AmpureXP beads (Agencourt) with a 1:1 (bead to sample) ratio to obtain library DNA products spanning 100-400 bp in length. Final libraries were quantified using Agilent Bioanalyzer 2100 and QuBit high-sensitivity dsDNA assay. Deep sequencing was performed by Illumina NextSeq 500 at CAS-MPG Partner Institute for Computational Biology Omics Core, Shanghai, China. About 15-25 million mapped sequencing reads were obtained for each sample, with 88% of bases at or above Q30.

Measurement of circRNA copy number

A serial dilution of purified DNA template of *circPOLR2A*-forming exons was used for qPCR to generate a standard curve. The copy number of the diluted DNA template was calculated by DNA/RNA Copy Number Calculator from the following website (<http://endmemo.com/bio/dnacopynum.php>). To measure the *circPOLR2A* copy per cell, total RNAs extracted from 1 × 10⁶ HeLa cells were reversely transcribed into cDNAs, and aliquots of cDNAs from 2,000 HeLa cells were fruther used for qPCR. The copy number of *circPOLR2A* was quantitated from the standard curve. Further, using the copy number and FPM of *circPOLR2A*, as well as FPM values of all detected circRNAs in HeLa cell RNA-seq datasets as references, we calculated the copy number of all detected circRNAs in control or RNase L KO HeLa cells before or after poly(I:C) stimulation (Tables S1 and S4). The copy number of overexpressed *circPOLR2A*, *circCAMSAP1* and *circSMRACA5* was also individually measured accordingly.

RNA Immunoprecipitation (RIP)

Cells growing in 10 cm dishes were rinsed twice with ice-cold PBS, harvested in 10 mL ice-cold PBS and then centrifuged at 1,000 rpm for 5 min at 4°C. Cells were resuspended in 1 mL RIP buffer (50 mM Tris, pH 7.4, 150 mM NaCl, 0.5% Igepal, 1 mM PMSF, 1X protease inhibitor cocktail (Roche) and 2 mM VRC) and subjected to three rounds of gentle sonication. Cell lysates were centrifuged at 12,000 rpm for 15 min at 4°C and the supernatants were precleared with 15 mL Dynabeads Protein G (Invitrogen) to get rid of non-specific binding. Then, the precleared lysates were used for IP with anti-Flag antibodies (Sigma) or anti-PKR antibodies (Abways). IP was carried out for 2 hr at 4°C. The beads were washed three times with high salt buffer and two times with the same RIP buffer, followed by extraction with elution buffer (100 mM Tris, pH 6.8, 4% SDS, and 10mM EDTA) at room temperature for 10 min. One-third of the eluted sample was used for WB and the remaining was used for RNA extraction. The RNA enrichment was assessed by qRT-PCR. Primers are listed in Table S5.

Cell proliferation assay

1 × 10⁴ WT, RNase L KO or PKR KO HeLa cells were seeded in 96-well, then cultured in 37° for 24h, and infected with EMCV (0.1 moi) for another 24h. Survival cells were measured according to CellTiter 96 AQueous One Solution Cell Proliferation Assay (Promega). Data were presented with respect to WT HeLa cells set to a value of 1.

Isolation of peripheral blood mononuclear cells (PBMCs) using Ficoll-Paque™

Whole blood samples from normal donors or SLE patients were collected and PBMCs were isolated by density-gradient centrifugation with Ficoll-Paque Premium (GE Healthcare). In brief, whole blood (10 mL) samples from individual normal donors or SLE patients were collected in collection tubes with 2-4 volumes of PBS. Then 35 mL of diluted cell suspension was layered over 15 mL of Ficoll-Paque in a 50 mL conical tube. After centrifuge at 400 g for 30-40 minutes at 20°C, the mononuclear cell layer was transferred to a new 50 mL conical tube and was filled with solution containing phosphate buffer (PBS with 2mM EDTA). After centrifugation at 200 g for 15 minutes at 20°C, PBMCs platelets were collected for use or storage in liquid nitrogen.

Isolation of monocytes, B cells and T cells from PBMCs

Individual PBMCs were isolated by density-gradient centrifugation with Ficoll-Paque Premium (GE Healthcare) as described above. Then CD14+ monocytes, CD19+ B cells and CD3+ T cells from individual PBMCs were separated using CD14, CD19 or CD3 microbeads (Miltenyi Biotec) according to the manufacturer's instructions. Isolated T cells, monocytes and B cells were collected for using or storage in liquid nitrogen.

Plasmid transfection to PBMCs and T cells isolated from SLE patients

For plasmid transfection, whole blood (10 mL) samples from individual SLE patients were collected and PBMCs were isolated (see above). CD3+ T cells were then sorted as described above by microbeads (Miltenyi Biotec) according to the manufacturer's instructions. Next, 1 × 10⁵ SLE patient-derived PBMCs and T cells were seeded in a 6-well plate and cultured in 37° for 24h. Individual plasmids were transfected into these cells using electroporation by Neon Transfection System (Invitrogen) with program X-001. The transfection efficiency was about 40% in general. Then total proteins and RNAs were harvested 24h after transfection.

Polyadenylated/non-polyadenylated RNA separation, rRNA depletion for RNA-seq

For RNA-seq samples from HeLa cells treated with poly(I:C) or EMCV (Figures 1, S2, and S3), polyadenylated [poly(A)+] and non-polyadenylated [poly(A)-/Ribo-] RNA preparation was carried out as previously described (Yang et al., 2011; Yin et al., 2015). Briefly, total RNAs (8 µg) were incubated with oligo(dT) magnetic beads to isolate either poly(A)+ RNAs, which were bound to beads, or non-polyadenylated RNAs, which were present in the flowthrough after incubation. Oligo(dT) magnetic bead selection was performed three times to ensure the purity of poly(A)+ or non-polyadenylated RNA populations. The non-polyadenylated RNA population was further processed with the RiboMinus kit (Human/Mouse Module, Invitrogen) to deplete ribosomal RNAs and to obtain poly(A)-/Ribo- (poly(A)- for simplicity) RNAs for sequencing.

Library preparation and deep sequencing

Ribo-, poly(A)+ and poly(A)- RNA-seq libraries were prepared using Illumina TruSeq Stranded Total RNA LT Sample Prep Kit. SHAPE-MaP libraries were prepared from 1 ng of DNAs reverse-transcribed from linearSHAPE or circSHAPE RNAs using Illumina TruSeq ChIP Sample Prep Kit. All libraries were size-selected with AmpureXP beads (Agencourt) and quantified using Agilent Bioanalyzer 2100 and QuBit high-sensitivity dsDNA assay. Size-selected libraries were subjected to deep sequencing with Illumina NextSeq 500 at CAS-MPG Partner Institute for Computational Biology Omics Core, Shanghai, China. Raw read qualities were evaluated by FastQC (<http://www.bioinformatics.babraham.ac.uk/projects/fastqc/>).

RtcB-ligase assisted qPCR

RNA fragments generated by RNase L were detected as described with a slight modification (Donovan et al., 2017). Briefly, total RNAs were purified by Trizol and RNAs with 2'-3' cyclic phosphate were ligated to the adaptor 5'rGrArUrCrGrUCGG ACTGTAGAACTCTGAAC 3' using RtcB RNA ligase. EDTA-quenched ligation reactions were reverse transcribed using

SuperScript II reverse transcriptase (Invitrogen) and the primer 5' TCCCTATCAGTGATAGAGAGTCAGAG TTCTACAGTCCG 3'. The resulting cDNAs were assessed for RNase L cleavage products by qPCR for specific cleavage sites and normalized to U6, which has a naturally occurring 2'-3' cyclic phosphate. The primers for RtcB-ligase assisted qPCR are listed in [Table S5](#).

QUANTIFICATION AND STATISTICAL ANALYSIS

RNA-seq analyses

Deep sequencing datasets were filtered by using Trimmomatic ([Bolger et al., 2014](#)) (parameters: PE -threads 16 -phred33 TruSeq3-PE-2.fa:2:30:10 LEADING:3 TRAILING:3 SLIDINGWINDOW:4:15 MINLEN:30) to remove low quality bases and adaptor sequences at both ends of reads.

Next, RNA-seq reads were uniquely aligned to rDNA sequences for pre-rRNAs (18S, 5.8S, 28S, and spacer regions) by Bowtie (bowtie version 0.12.9, parameters: -m 1 -k 1 -v 2 -p 12 -S) to remove reads mapped to rDNA regions, and then aligned to GRCh37/hg19 human reference genome with the UCSC Genes annotation (Human: hg19 knownGene.txt updated at 2013/6/30) by HISAT2 ([Kim et al., 2015](#)) (version 2.0.5, parameters: --known-splicesite-infile --no-softclip --rna-strandness RF --score-min L,-16,0 --mp 7,7 --rdg 0,7 --max-seeds 20 -k 10 -t -p 12 -S). Gene expression of linear mRNAs was determined by FPKM (Fragments Per Kilobase of transcript per Million mapped reads) with RSeQC (version 2.6.4, default parameters). The maximum FPKM of expressed transcripts of a given gene was selected to represent the expression level of this gene. Expression of linear mRNAs in HeLa cells under different conditions was listed in [Tables S1, S2, S3](#), and [S4](#), and expression of linear mRNAs in SLE patients and control normal donors was listed in [Table S6](#).

Of note, RNA-seq datasets from EMCV treated cells were first aligned to EMCV virus genome sequence by HISAT2 ([Kim et al., 2015](#)) (version 2.0.5, parameters: --known-splicesite-infile --no-softclip --rna-strandness RF --score-min L,-16,0 --mp 7,7 --rdg 0,7 --max-seeds 20 -k 10 -t -p 12 -S) to remove reads mapped to EMCV virus genome.

CircRNA expression was then determined by CIRCexplorer2 as previously reported ([Zhang et al., 2016a](#)). Briefly, unmapped reads were realigned to GRCh37/hg19 human reference genome using TopHat-Fusion ([Kim and Salzberg, 2011](#)) (TopHat v2.0.12, parameters: --fusion-search --keep-fasta-order --bowtie1 --no-coverage-search) to obtain reads mapped to back-splicing junction (BSJ) sites. CircRNAs were then predicted with existing gene annotations (Human GRCh37/hg19 known Gene.txt updated at 2013/6/30 and refFlat.txt updated at 2017/04/09) as previously described ([Zhang et al., 2016a](#)). Expression of circRNAs was evaluated by FPM (Fragments mapped to back-splicing junctions Per Million mapped fragments) ([Zhang et al., 2016a](#)). High-confidence circRNAs were determined with $FPM \geq 0.2$ in at least one sample. Identified circRNAs in HeLa cells upon different treatments were listed in [Tables S1, S2, S3](#), and [S4](#).

Finally, for RNA-seq in SLE and control samples, overlapped circRNAs were identified by $FPM > 0$ in monocytes, B cells and T cells in control donor samples. Then, the fold change (FC) of each circRNA was defined by upregulated ($FC \geq 2$), unchanged ($0.5 < FC < 2$) or downregulated ($FC \leq 0.5$) one in SLE, compared to that in control samples in all three types of immune cells. Meanwhile, the FC of each corresponding linear mRNA was determined in these three types of immune cells from SLE and controls. All identified circRNAs and their linear cognate mRNAs in SLE and control samples were listed in [Table S6](#).

SHAPE reactivity calculation

SHAPE reactivity profiles were created from deep sequencing datasets for linear or circular RNAs using ShapeMapper software (v2.1.3) ([Busan and Weeks, 2018](#)) with modified parameters (-target RNA.fa --out folder --nproc 16 --verbose --serial --min-depth 50 --modified --untreated --denatured). Deep sequencing reads with low quality scores were trimmed. Then paired-end reads without overlapping sequences were analyzed as two single reads, while paired-end reads with overlapping sequences were combined to single reads. Pre-processed reads were then mapped to target sequences by Bowtie2 (v2.1.0) (-p 24 --local --sensitive-local --mp 3,1 --rdg 5,1 --rfg 5,1 --dpad 30 --maxins 800 --ignore-quals --no-unal). Mutation rates (MutR) were calculated at each position by summing the number of mismatches and indels (deletions and insertions) and divided by the number of all mapped reads to the position. SHAPE reactivities were calculated by $[(\text{Modified}_{\text{MutR}} - \text{Untreated}_{\text{MutR}})/\text{Denatured}_{\text{MutR}}]$ and further normalized by a model-free box-plot approach ([Deigan et al., 2009](#)).

Different from the standard pipeline by ShapeMapper software (v2.1.3) ([Busan and Weeks, 2018](#)) for linear RNA SHAPE-MaP analysis, two rounds of mapping were performed with reads from circSHAPE-MaP libraries. After the first round of mapping by Bowtie2 with aforementioned parameters, soft clipping reads were identified. These clipped sequences were then combined with the first-round mapped reads for re-alignment by Bowtie2 to retrieve a better mapping efficiency at back-splicing junction sites for circRNAs. Mapped read sequences that match PCR primer sequences, if located at 5' ends of mapped reads, were removed for subsequent SHAPE reactivity profiles. Source codes for circSHAPE-MaP analysis are available at <https://github.com/YangLab/CIRCshapemapper>.

RNA secondary structure modeling

An initial list of a total 38 pairs of circRNAs and linear RNAs for in-cell SHAPE-MaP-seq were designed with expected PCR products of ~300 bp for circRNAs and ~700 bp for linear RNAs. However, 700 bp PCR products for linear RNAs after NAI probing could not yield enough coverage for analysis (100 × depth with 70% coverage, [Figure S5A](#)). Then, 15 linear RNAs for in-cell SHAPE-MaP-seq

were designed with expected PCR products of ~300 bp for linear RNAs, the same length as those in circRNAs in-cell SHAPE-MaP-seq (Figure S5B).

After sequencing, reactive positions with more than $100 \times$ depth in all three (modified, untreated and denatured) samples were selected for mutation rate calculation (Busan and Weeks, 2018). > 80% positions covered more than 100 reads for circRNAs and > 70% positions covered more than 100 reads for linear RNAs were called to filter reliable SHAPE-MaP-seq reads from duplicated experiments (Figures S5A and S5B). 12 of 15 linear RNAs passed these parameters and were used in this study (Figure S5B). 26 of 38 circRNAs without paired linear RNA in-cell SHAPE-MaP-seq were further analyzed > 80% positions covered more than 1000 reads and 22 circRNAs passed the filters (Figure S5C).

With these SHAPE reactivities values for different RNAs, RNA secondary structures were modeled by RNAfold (v2.4.2) (Lorenz et al., 2011) with different parameters for linear (-p -d2 --shape=SHAPE profile --shapeMethod=D) or circular (-p -d2 --shape=SHAPE profile --shapeMethod=D --circ) (Hofacker and Stadler, 2006) RNAs.

Double-stranded RNA structure analysis

Double-stranded RNA (dsRNA) structures were identified from modeled RNA secondary structures by RNAfold. Length (base pair, bp) of each dsRNA was determined by the length of the shorter strand sequence. In this study, dsRNAs with at least 16 bp in length, with bulges and inter-loops ≤ 4 nucleotides (nt), were further analyzed (Figure 3E). Base pairing probability (Figure 3E) of a dsRNA was calculated by averaging pairing probability of all paired bases, which was determined by RNAfold during RNA secondary structure modeling.

Structural models of all circRNAs shown in Figures 3–4 and Table 1 were calculated from the circSHAPE-MaP replicate 1. In total, the 26 dsRNA-containing circRNAs listed in Table 1 displayed 48 dsRNA regions as revealed by circSHAPE-MaP replicate 1 (Figures 3 and 4) and 45 dsRNA regions revealed by the replicate 2 (data not shown). 12 paired linear RNAs shown in Figures 3D–3F and Table S5 were calculated from the averaged SHAPE-MaP values of two replicates.

Three-dimensional RNA structure modeling

The 3D structure of *circPOLR2A* was modeled by 3dRNA (v2.0) (Wang et al., 2017; Zhao et al., 2012) (<http://biophy.hust.edu.cn/3dRNA/>) with the inputs of primary sequence and modeled secondary structure (in the dot-bracket form) of *circPOLR2A* by RNAfold.

Statistical analyses

Statistical significance for comparisons of means was generally assessed by Student's t test with exceptions described below. $p < 0.05$ were marked by 1 asterisk, while 2 asterisks indicate a $p < 0.01$ and 3 asterisks a $p < 0.001$. Statistically significant difference for RNA-seq was assessed by Wilcoxon rank-sum test (R v.3.2.2), and statistical significance was set at $p < 0.05$. To evaluate the relevant correlations between two group datasets (Figure 3C), Spearman's rank correlation coefficient between two biological replicates of 12 pairs of circRNAs and their linear cognate RNAs was performed with R platform (R v.3.2.2). Statistically significant difference for pairing probability (Figure 3E) was assessed by F test, and statistical significance was set at $p < 0.05$.

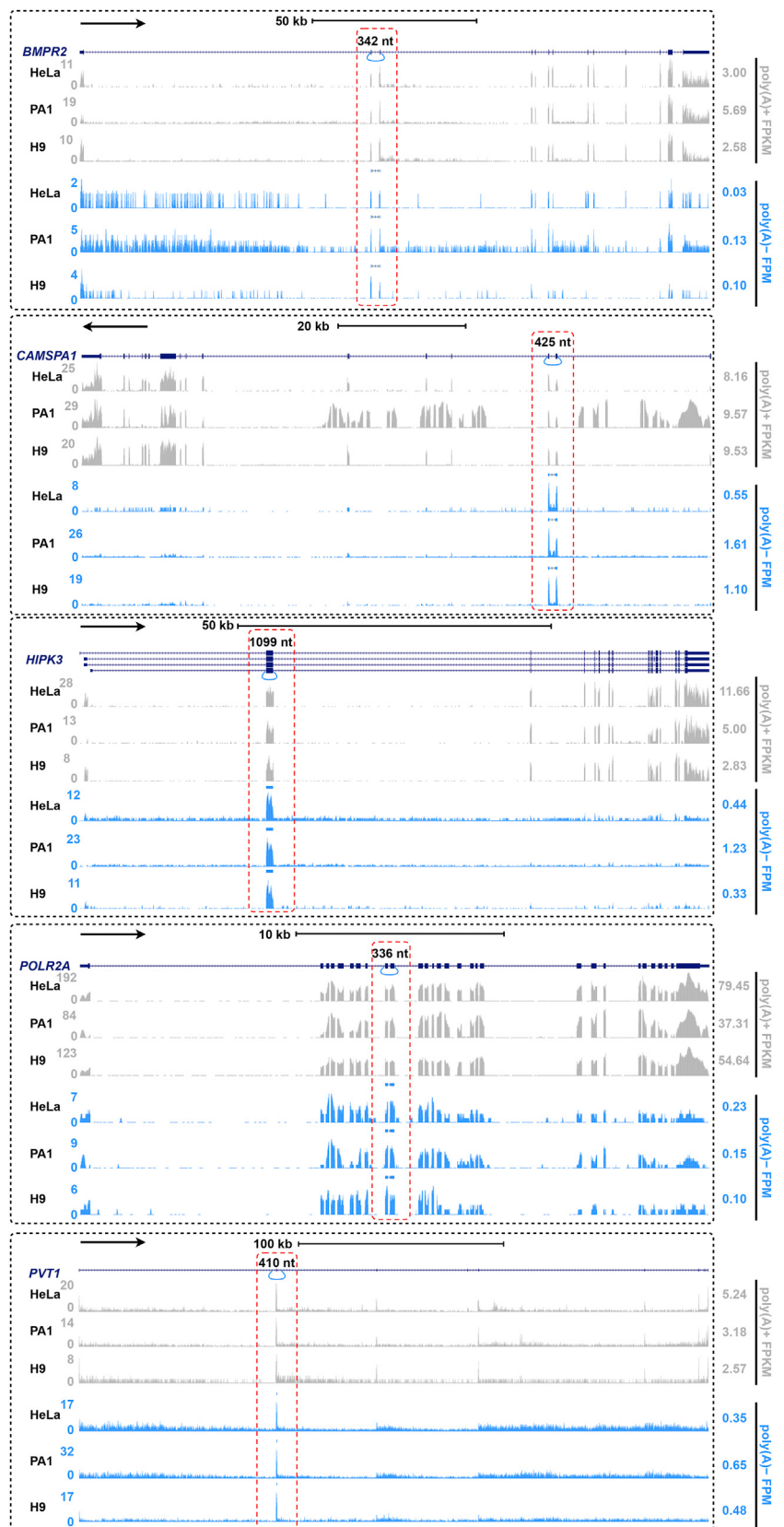
DATA AND SOFTWARE AVAILABILITY

All sequencing data reported in this paper have been deposited in the GEO (Gene Expression Omnibus) and NODE (National Omics Data Encyclopedia). The accession numbers for linear and circular RNA expression in HeLa cells are GEO: GSE122967 and NODE: OEP000216, for SHAPE reactivity of linear and circular RNAs are GEO: GSE126195 and NODE: OEP000216, and for linear and circular RNA expression in normal and SLE donors is NODE: OEP000216. Structural models of paired circRNAs and linear cognates from individual SHAPE-MaP replicates can be accessed at <http://www.picb.ac.cn/rnomics/circSHAPE-MaP>.

All original unprocessed data related to this paper were uploaded to Mendeley Data in the website: <https://doi.org/10.17632/bs6fz5m5th.1>.

Supplemental Figures

Cell



(legend on next page)

Figure S1. Gene Organization of circRNAs, Related to Figure 1

The gene organization of five examined circRNAs, *circBMPR2*, *circCAMSAP1*, *circHIPK3*, *circPOLR2A* and *circPVT1* are shown. The origin of exons, their expression levels from the poly(A)- RNA-seq (blue wiggle tracks), and the expression of their cognate mRNAs from the poly(A)+ RNA-seq (gray wiggle tracks) in HeLa cells (Li et al., 2017), human embryonic carcinoma cells PA1 (Zhang et al., 2016b) and human embryonic stem cells H9 (Zhang et al., 2014) are shown.

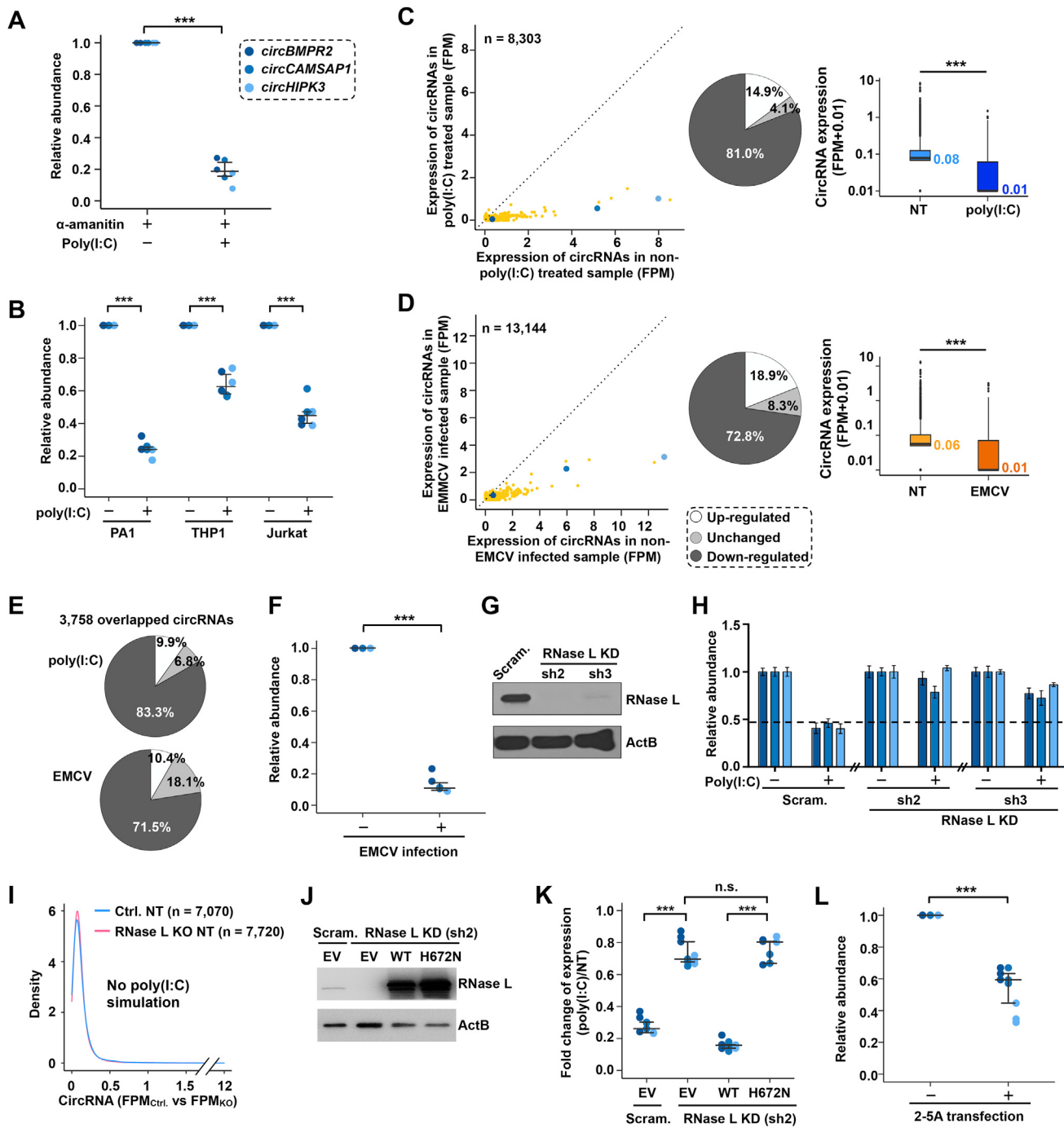


Figure S2. circRNAs Undergo Degradation by RNase L in Cells upon Poly(I:C) or EMCV Treatment, Related to Figure 1

(A) CircRNAs are rapidly degraded upon poly(I:C) treatment after the addition of α -amanitin to block transcription. HeLa cells were treated with α -amanitin for 6h prior to poly(I:C) treatment for 2h, and the relative abundance of circRNAs were measured by qRT-PCR.

(B) CircRNAs are degraded upon poly(I:C) treatment. PA1, THP1 or Jurkat cells were treated with poly(I:C) for 6h and the relative abundance of circRNAs were measured by qRT-PCR. The transfection of poly(I:C) to PA1 cells was about only 80%, compared to about 40% in THP1 cells and 50% in Jurkat cells (data not shown).

(C) (D) Global circRNA degradation in cells treated with poly(I:C) (C) or EMCV (D). poly(A)- RNA-seq followed by the identification of steady-state circRNAs revealed a global reduction of circRNAs upon poly(I:C) treatment for 6h (C) or EMCV infection for 24h (D). Left, a scatterplot shows all circRNA expression between untreated cells and cells upon poly(I:C) treatment (C) or EMCV infection (D) and circRNAs in (A) are highlighted. Middle, pie charts showing upregulated (fold change ≥ 2), unchanged (0.5 $<$ fold change < 2) and downregulated (fold change ≤ 0.5) circRNAs. EMCV, encephalomyocarditis virus. Right, boxplots show circRNA expression changes between untreated cells and cells upon poly(I:C) treatment (C) or EMCV infection (D).

(legend continued on next page)

-
- (E) Expression of overlapped circRNAs shown in (C) and (D) is largely decreased upon poly(I:C) or EMCV treatment. Pie charts show upregulated (fold change ≥ 2), unchanged ($0.5 < \text{fold change} < 2$) and downregulated (fold change ≤ 0.5) circRNAs.
- (F) Validation of circRNA degradation upon EMCV infection for 24h in HeLa cells.
- (G) RNase L knockdown (KD) by two different shRNAs in HeLa cells confirmed by Western Blotting (WB).
- (H) RNase L is responsible for circRNAs degradation upon poly(I:C) treatment. CircRNA degradation was largely rescued in RNase L KD HeLa cells upon poly(I:C) treatment. Error bars represent standard deviation.
- (I) The expression of circRNAs showed subtle changes in control and RNase L KO HeLa cells without poly(I:C) treatment.
- (J) WB confirmed the expression of RNase L (WT) and its nuclease-dead mutation (H672N) in RNase L KD HeLa cells. EV, empty vector.
- (K) The endonuclease activity of RNase L is required for the rapid degradation of circRNAs upon poly(I:C) treatment. Decreased circRNA levels shown in Figure 1A upon poly(I:C) treatment could be restored by re-introduction of WT RNase L, but not its catalytically inactive mutant H672N, into RNase L KD cells.
- (L) CircRNAs are degraded upon 2-5A transfection in HeLa cells. Transfection of 2-5As into HeLa cells for 12h to activate RNase L led to reduced circRNA expression. 2-5As, 2', 5'-linked oligoadenylates of variable length.
- (A)(B)(F)(K)(L), data are shown as median and interquartile range (IQR). n.s., $p > 0.05$, ** $p < 0.01$, *** $p < 0.001$, Student's t test.
- (C)(D), the median, IQR and $1.5 \times \text{IQR}$ are shown. *** $p < 0.001$, Wilcoxon rank-sum test.

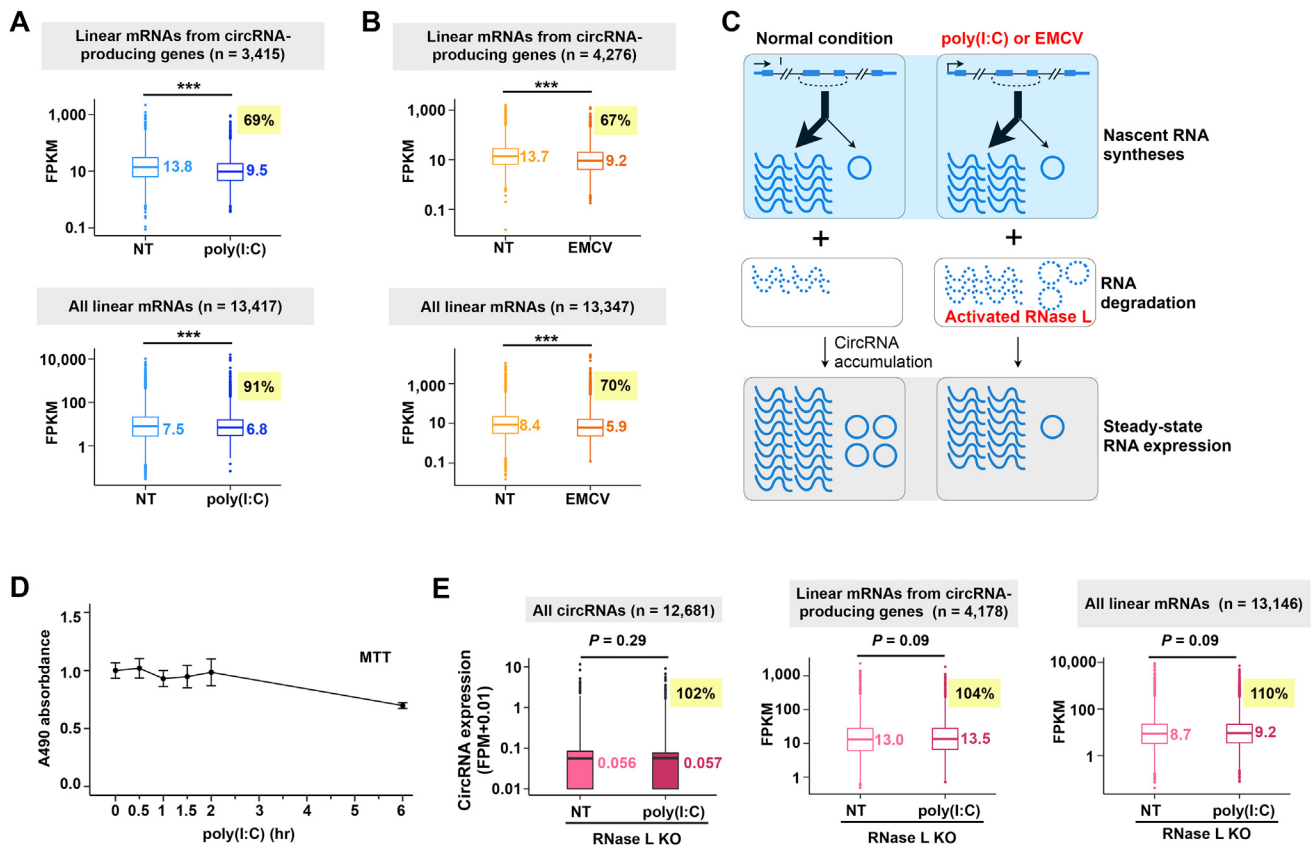


Figure S3. Linear mRNA Degradation upon Poly(I:C) or EMCV Treatment, Related to Figure 1

(A) Cellular linear mRNAs are cleaved upon poly(I:C) treatment. Linear RNAs from circRNA-producing genes (top) or all linear mRNAs (bottom) were reduced to 69% or 91%, respectively upon poly(I:C) treatment for 6h.

(B) Cellular linear mRNAs are cleaved upon EMCV infection. Linear RNAs from circRNA-producing genes (top) or all linear mRNAs (bottom) were reduced to 67% or 70%, respectively upon EMCV infection for 24h.

(C) A schematic drawing of circRNA biogenesis, degradation and accumulation in normal (left), or poly(I:C) or EMCV-treated condition (right).

(D) MTT assays to show cell viability upon poly(I:C) treatment at indicated time points. HeLa cells remained 100% viable within 2h and 80% within 6h of poly(I:C) treatments. Error bars represent standard deviation.

(E) All circRNAs (left), linear RNAs from circRNA-producing genes (middle) or all linear mRNAs (right) remain largely unchanged in RNase L KO HeLa cells upon poly(I:C) stimulation.

(A) (B) (E), the median, IQR and $1.5 \times$ IQR are shown. n.s, p > 0.05, **p < 0.01, ***p < 0.001, Wilcoxon rank-sum test.

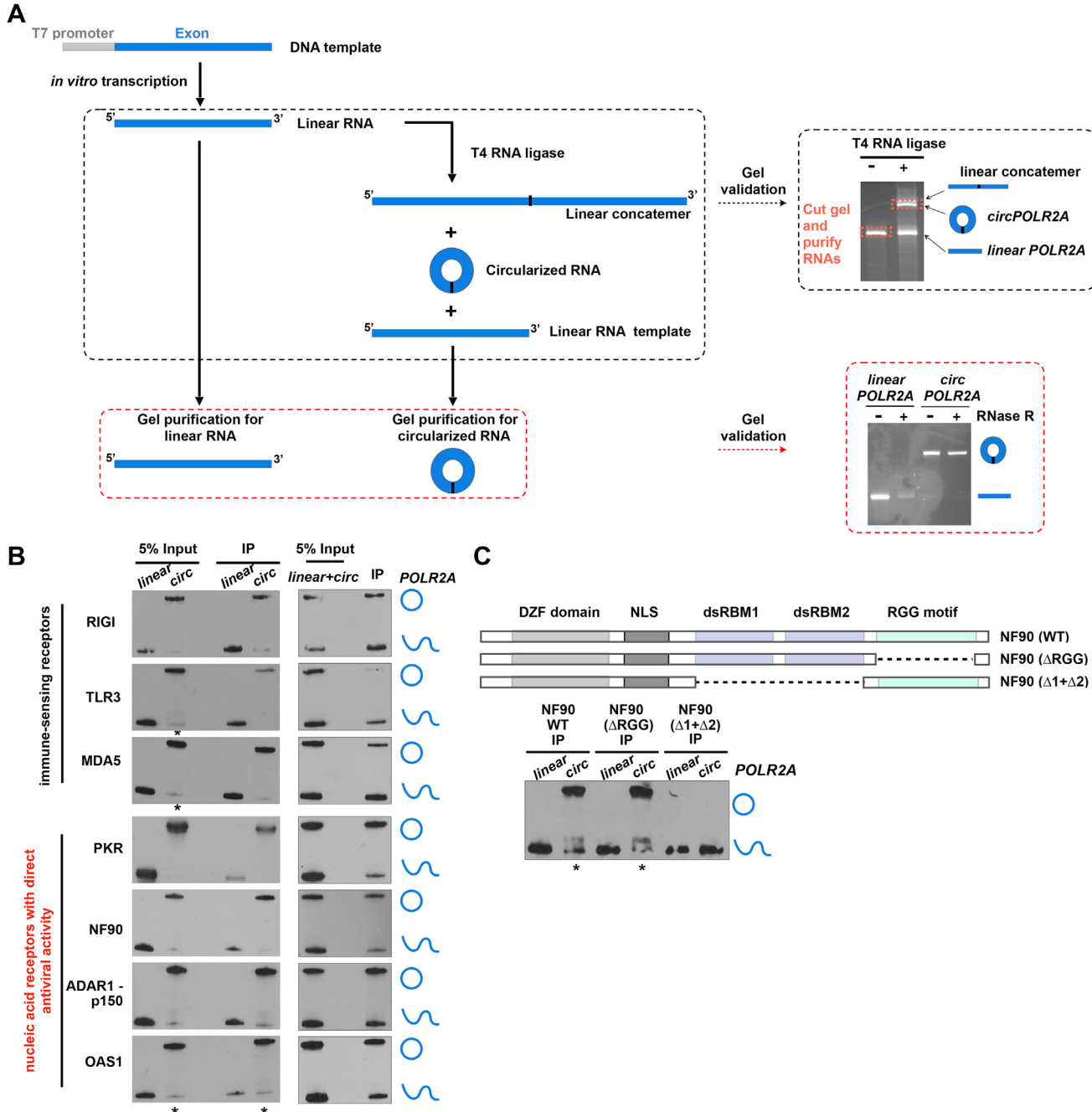


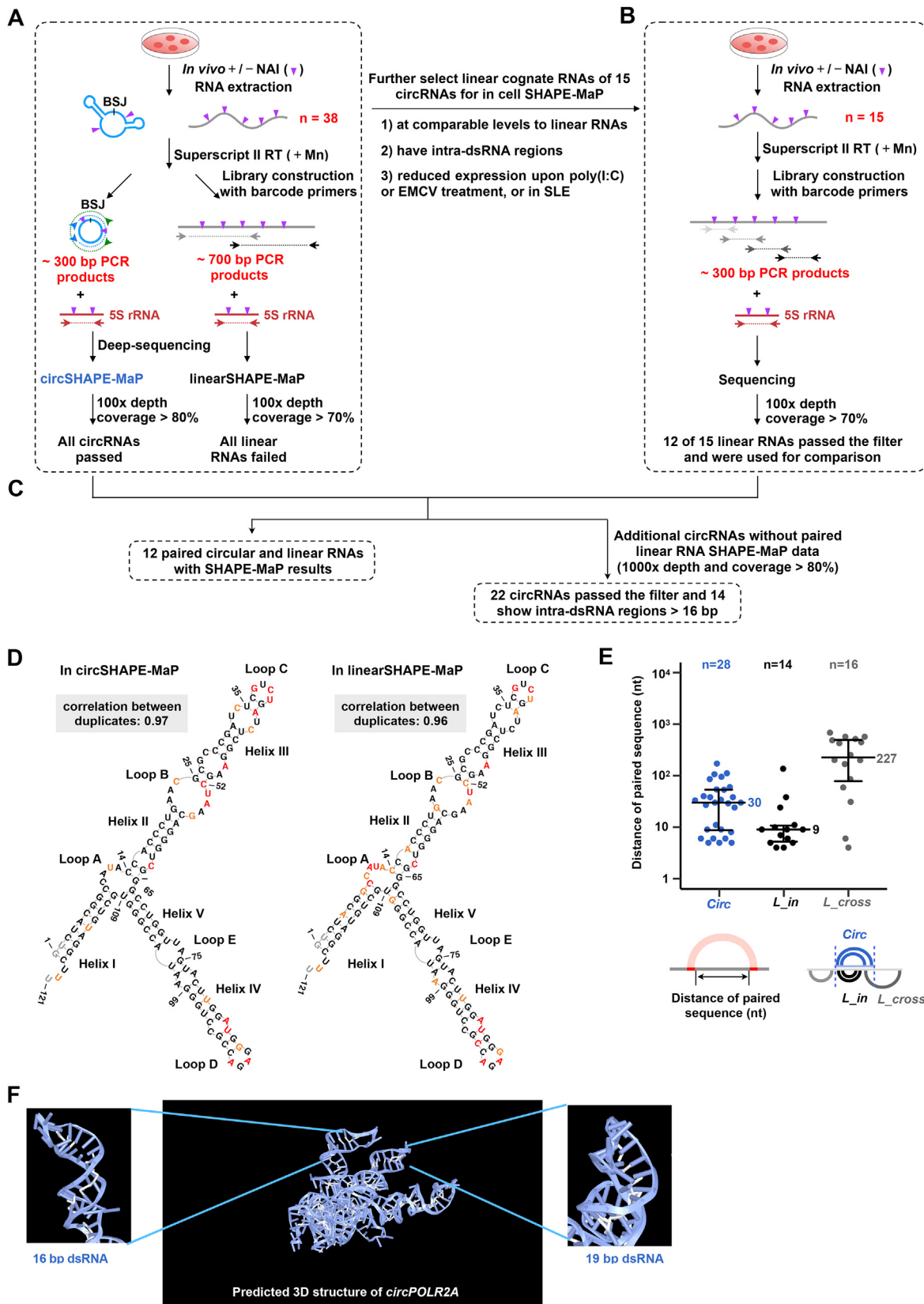
Figure S4. circRNAs Preferentially Bind to Nucleic Acid Receptors with Antiviral Activity, Related to Figure 2

(A) A schematic drawing to show *in vitro* circularization and purification of circular and linear RNAs, using *circPOLR2A* and linear *POLR2A* as examples. Left, an illustration shows that an expression vector produces linear RNAs, which are further treated with T4 RNA ligase to generate circular RNAs. Right, stepwise purification of linear RNAs and circular RNAs. Circular and linear RNAs were purified via denaturing PAGE gel and purification (top right). Circular RNAs were confirmed by RNase R digestion (bottom right).

(B) CircRNAs preferentially bind to nucleic acid receptors with antiviral activity, shown by both *in vitro* binding (left) and competition (right) assays. See Figures 2A and 2B for details.

(C) DsRNA-binding motifs (dsRBMs) in NF90 are critical for *circPOLR2A* binding. Top, a schematic drawing of NF90 and its truncation without two dsRBMs. Bottom, the NF90 dsRBM truncation, but not its RGG truncation, is no longer bound to *circPOLR2A*.

(B) and (C). * indicates linearized circRNAs during experimental procedures *in vitro*.



(legend on next page)

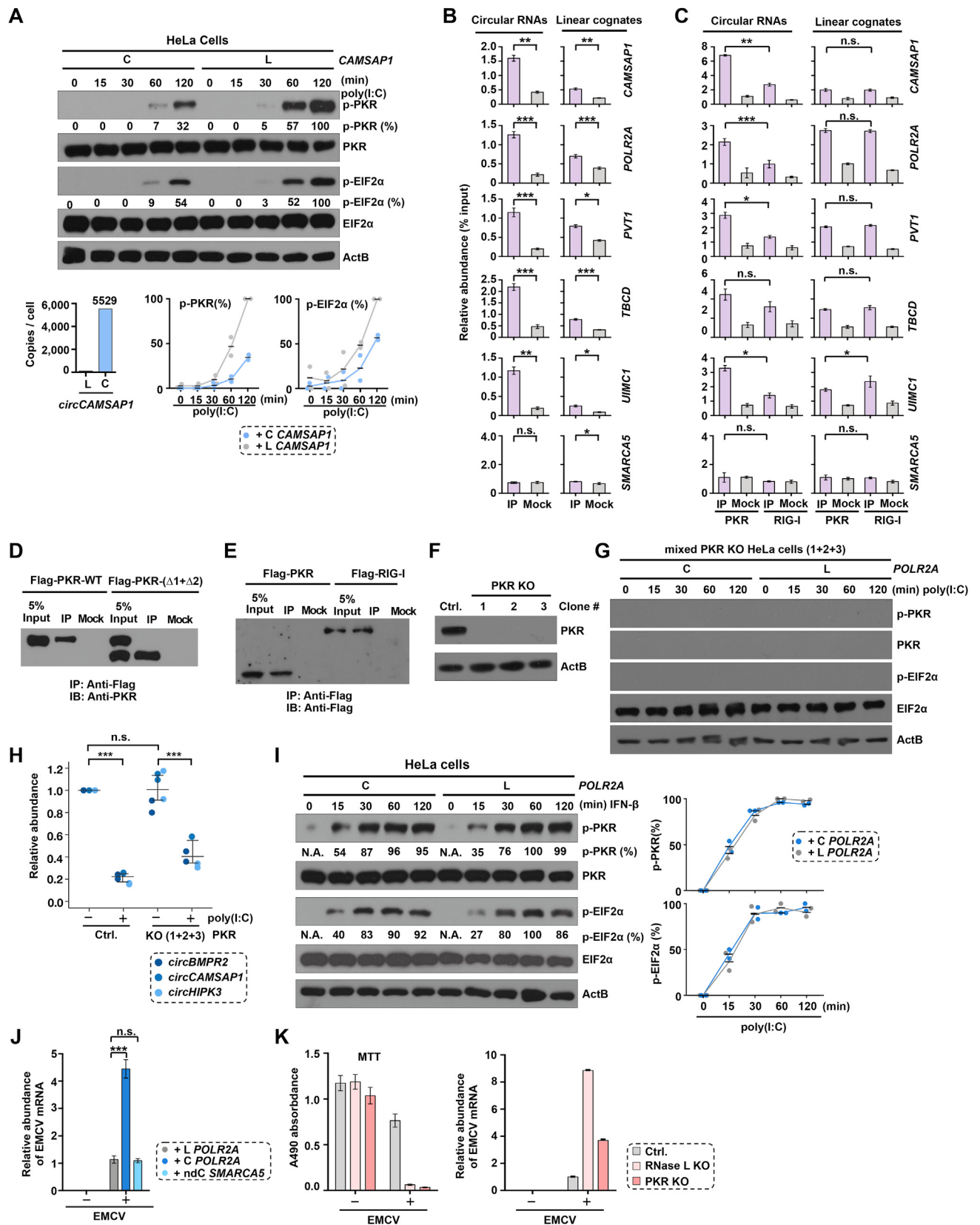
Figure S5. Overview of SHAPE-MaP for Examined circRNAs, Related to Figures 3 and 4 and Table 1

(A)(B)(C) An illustration shows the strategy for library construction and computational analyses of SHAPE-MaP datasets.

(D) Secondary structural models of human 5S rRNA revealed in circSHAPE-MaP and linearSHAPE-MaP. Red, orange and black colors are corresponding to high, moderate and low reactivities, respectively. Spearman's rank correlation coefficient of human 5S rRNA is high in circSHAPE-MaP (0.97) and linearSHAPE-MaP (0.96) assays, suggesting that these SHAPE reactivities were highly reproducible.

(E) Distances between paired sequences for dsRNA duplexes (length \geq 16 bp) in all examined circular and linear RNAs. Top, distances for potential dsRNA duplexes in linear RNAs were longer than those in circular RNAs. Blue dots indicate potential dsRNA duplexes found in circular RNAs; black dots indicate potential dsRNA duplexes found in linear RNAs within circRNA-forming sequence regions (L_{in}); gray dots indicate potential dsRNA duplexes found in linear RNAs beyond circRNA-forming sequence regions (L_{cross}). Bottom, two drawings show how the distance of dsRNA duplexes was calculated and how $Circ$, L_{in} and L_{cross} were determined in a circRNA or the paired linear RNA. Data are shown as median and IQR.

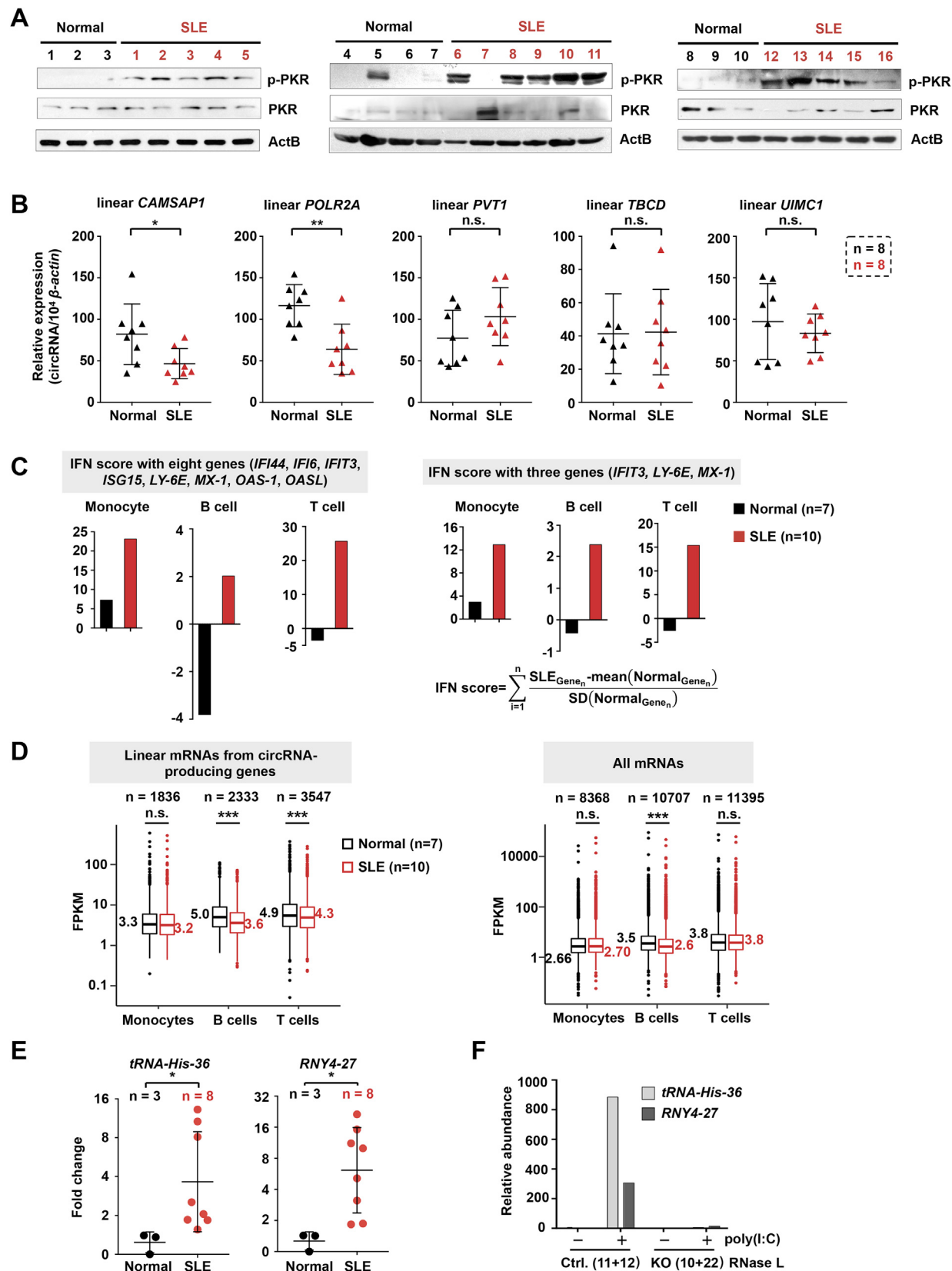
(F) A three-dimensional model of *circPOLR2A* with the secondary structures revealed by the SHAPE reactivities. Two dsRNA regions with 16 and 19 bp (Figure 3D) and a three-dimensional model of the full-length *circPOLR2A* were shown (3D model was illustrated by 3dRNA v2.0).



(legend on next page)

Figure S6. circRNAs Block PKR Phosphorylation and RNase L/PKR Are Essential for Cells to Prevent Viral Replication, Related to Figure 5

- (A) Overexpression of *circCAMSAP1*, but not linear *CAMSAP1*, in HeLa cells inhibits PKR phosphorylation (p-PKR-T446, p-PKR for simplicity) upon poly(I:C) stimulation. WT cells and cells transfected with vectors shown in Figure 4C that contain circle-forming exons of *CAMSAP1* for 24h, followed by poly(I:C) treatment at indicated time points. Left, levels of PKR, p-PKR, EIF2 α , p-EIF2 α -S51 (p-EIF2 α for simplicity) and ActB in these cells. The transfection and WBs were performed twice with similar results and quantification was shown on the bottom right. Bottom left, the copy number of the overexpressed *circCAMSAP1* per cell was shown.
- (B) PKR is associated with intra-dsRNA-containing circRNAs in cells. Anti-PKR or anti-IgG (Mock) was used to precipitate associated RNAs in HeLa cells, respectively. The percentage of RIP-enriched circular and linear cognate RNAs relative to input was calculated under each condition.
- (C) Flag-PKR, but not Flag-RIG-I, is associated with intra-dsRNA-containing RNAs in cells. HeLa cells stably expressing Flag-PKR or Flag-RIG-I were subjected to RIP using anti-Flag (IP) or anti-IgG (Mock) antibodies, respectively. The percentage of RIP-enriched circular and linear cognate RNAs relative to input was calculated under each condition.
- (D) Both Flag-PKR and Flag-PKR-(Δ1+2) were overexpressed at similar levels in HeLa cells and anti-Flag pull-down efficiencies were comparable. Proteins collected from Input, IP and Mock were detected by WB using anti-Flag antibodies.
- (E) Both Flag-PKR and Flag-RIG-I were overexpressed at similar levels in HeLa cells and anti-Flag pull-down efficiencies were comparable. Proteins collected from Input, IP and Mock were detected by WB using anti-Flag antibodies.
- (F) Generation of PKR knockout (KO) cell lines by CRISPR/Cas9 in HeLa cells. Clones of control HeLa cells (Ctrl.) and PKR KO cell lines were obtained, and confirmed by WB. To limit the heterogeneity between three PKR KO single cell clones, three PKR KO lines were mixed for experiments carried out in (G) and (K).
- (G) Phosphorylation of PKR and EIF2 α was no longer detected upon poly(I:C) in PKR KO cells, regardless of the addition of circular or linear RNAs expression. Transfection and WB were performed twice with similar results.
- (H) PKR is not required for the circRNA degradation upon poly(I:C) treatment. CircRNA reduction upon poly(I:C) treatment in WT cells was comparable to that in PKR KO HeLa cells. Data are shown as median and IQR. n.s., p > 0.05, ***p < 0.001, Student's t test.
- (I) circRNAs do not compete for the cytokine (IFN-β) induced PKR activation. Left, HeLa cells were transfected with vectors that express either *circPOLR2A* or linear cognate RNAs only (Figure 4C) for 24h, followed by IFN-β treatment at indicated time courses and WB detection of PKR, p-PKR, EIF2 α , p-EIF2 α and ActB in these cells. Transfection and WB were performed twice with similar results and quantification was shown on right.
- (J) Overexpression of circRNAs facilitates viral replication in HeLa cells. Linear or circular *POLR2A* or *circSMARCA5* was overexpressed by individual plasmids shown in Figure 5C in HeLa cells for 24h, followed by EMCV infection 24h and the detection of EMCV mRNAs by qRT-PCR.
- (K) Loss of RNase L or PKR facilitates viral replication in HeLa cells. Left, loss of RNase L or PKR led to significant cell death upon EMCV infection, as revealed by MTT assays. Right, loss of RNase L or PKR facilitates viral replication in HeLa cells, as revealed by the increased EMCV mRNA levels in RNase L or PKR KO HeLa cells 24h upon EMCV infection.
- (A)(I), the level of p-PKR and p-EIF2 α in each panel was quantified by Quantity One. p-PKR and p-EIF2 α levels were normalized by PKR or EIF2 α expression, respectively. Each dot represents the result from one experiment under each condition.
- (B)(C)(H)(J), error bars represent standard deviation in three independent experiments. Error bars represent standard deviation. n.s., p > 0.05, *p < 0.05, **p < 0.01, ***p < 0.001, Student's t test.
- (K), error bars represent SD.



(legend on next page)

Figure S7. PKR Phosphorylation and circRNA-Cognate Linear mRNA Expression in SLE Patients, Related to Figure 6

(A) PKR phosphorylation is generally augmented in PBMCs derived from individual SLE patients ($n = 16$), compared to that in cells from matched normal donors ($n = 10$), as revealed by WB of the total PKR and phosphorylated PKR (p-PKR).

(B) circRNA-cognate linear mRNA expression in PBMCs derived from individual SLE patients, compared to those from normal donors. The expression of circRNAs was examined in [Figure 5B](#). * $p < 0.05$, ** $p < 0.01$, Student's t test, error bars represent standard deviation.

(C) IFN scores of three major types of immune cells (monocytes, B cells and T cells) from SLE and normal donors. Eight (*IFI44, IFI6, IFIT3, ISG15, LY-6E, MX-1, OAS-1, OASL*) or three (*LY-6E, MX-1, IFIT3*) IFN-inducible genes were used to calculate the IFN scores.

(D) Expression of linear RNAs in monocytes, B cells and T cells isolated from PBMCs of normal and SLE samples. CircRNA-cognate linear RNAs (left) or all linear RNAs (right) from SLE patient samples were slightly decreased in B cells. The median, IQR and $1.5 \times$ IQR are shown. n.s., $p > 0.05$, *** $p < 0.001$, Wilcoxon rank-sum test.

(E) Subtle RNase L activation detected by RtcB-qPCR in PBMCs isolated from SLE patients. Expression of RNase L cleavage products including tRNA-His-36 and RNY4-27 was increased in PBMCs isolated from SLE patients, compared to those from normal donors. * $p < 0.05$, Student's t test, error bars represent SD.

(F) Strong RNase L activation detected by RtcB-qPCR upon poly(I:C) stimulation in HeLa cells. WT or RNase L KO HeLa cells were treated with poly(I:C) for 6h followed by the collection of total RNAs for RtcB-qPCR. Expression of RNase L cleavage products including tRNA-His-36 and RNY4-27 strongly appeared in WT HeLa cells upon poly(I:C) stimulation, but barely detected in RNase L KO cells.